CO2MVS RESEARCH ON SUPPLEMENTARY OBSERVATIONS

D3.4 Final and complete version of the APO and 14CO2 flux databases

Due date of Deliverable	31/12/2024
Submission date	07/01/2024; revised version 13/02/2025
File Name	CORSO-D3-4-V1.1
Work Package /Task	WP3 / T3.2
Organisation Responsible of Deliverable	TNO
Author name(s)	Marya el Malki, Hugo Denier van der Gon, Hannah Allen, Grégoire Broquet, Carlos Gomez, Marko Scholze, Eric Saboya, Philippe Ciais, Claire Granier, Antoon Visschedijk
Revision number	V1.1
Status	Issued
Dissemination Level / location	Public

The CORSO project (grant agreement No 101082194) is funded by the European Union.

1. Guidance for the reader/Executive Summary

This document presents the work done for deliverable D3.4: Final and complete version of the atmospheric potential oxygen (APO) and $^{14}CO2$ flux databases, under Work Package 3, Task 3.2 of CORSO. It highlights the collective work accomplished by the task partners and describes the final datasets now available for users. This includes the following:

1. Data for terrestrial and oceanic isotopic disequilibrium fluxes and nuclear emissions by Lund University and LSCE:
    a. The nuclear emissions and ocean disequilibrium data can be accessed on the GitHub repository.
    b. For the terrestrial fluxes, a more detailed description and accompanying papers are available on the CORSO project website and the data is available upon request by contacting Marko Scholze (marko.scholze@nateko.lu.se).
    c. The terrestrial data can be accessed here.

2. Global and regional ocean flux databases by the University of Bristol:
    a. Jena Carboscope available here.
    b. CESM2-FOSI available here.
    c. Bottom-Up fluxes available here.
    d. NEMO-ERSEM (v1.7) available here.
    e. ECCO-Darwin available here.

3. Regional anthropogenic APO_v3 inventory by TNO available in the following FTP repository:

    CORSO

    - Host: web-ftp81.tno.nl
    - Protocol: FTP
    - Encryption: Require explicit FTP over TLS
    - Logon type : normal
    - User : CORSO@ftp0015.web-ftp81
    - Password: 4NVdConP4Yw7

4. Future APO emissions based on IPCC AR6 SSP1 scenario for the years 2030 and 2050 will be made available around 15 February 2025 on the same FTP repository as mentioned above for the Regional anthropogenic APO_v3 inventory by TNO.

Each section encapsulates the methodologies adopted by the different groups, provides results and points the user to the datasets. For additional information or clarification, contact details are provided within the respective sections.

Table of Contents

2. Introduction

2.1. Background

To enable the European Union (EU) to move towards a low-carbon economy and implement its commitments under the Paris Agreement, a binding target was set to cut emissions in the EU by at least 40% below 1990 levels by 2030. European Commission (EC) President von der Leyen committed to deepen this target to at least 55% reduction by 2030. This was further consolidated with the release of the Commission's European Green Deal on the 11th of December 2019, setting the targets for the European environment, economy, and society to reach zero net emissions of greenhouse gases in 2050, outlining all needed technological and societal transformations that are aiming at combining prosperity and sustainability. To support EU countries in achieving the targets, the EU and European Commission (EC) recognised the need for an objective way to monitor anthropogenic CO2 emissions and their evolution over time.

Such a monitoring capacity will deliver consistent and reliable information to support informed policy- and decision-making processes, both at national and European level. To maintain independence in this domain, it is seen as critical that the EU establishes an observation-based operational anthropogenic CO2 emissions Monitoring and Verification Support (MVS) (CO2MVS) capacity as part of its Copernicus Earth Observation programme.

The CORSO research and innovation project will build on and complement the work of previous projects such as CHE (the CO2 Human Emissions), and CoCO2 (Copernicus CO2 service) projects, both led by ECMWF. These projects have already started the ramping-up of the CO2MVS prototype systems, so it can be implemented within the Copernicus Atmosphere Monitoring Service (CAMS) with the aim to be operational by 2026. The CORSO project will further support establishing the new CO2MVS addressing specific research & development questions.

The main objectives of CORSO are to deliver further research activities and outcomes with a focus on the use of supplementary observations, i.e., of co-emitted species as well as the use of auxiliary observations to better separate fossil fuel emissions from the other sources of atmospheric CO2. CORSO will deliver improved estimates of emission factors/ratios and their uncertainties as well as the capabilities at global and local scale to optimally use observations of co-emitted species to better estimate anthropogenic CO2 emissions. CORSO will also provide clear recommendations to CAMS, ICOS, and WMO about the potential added-value of high-temporal resolution 14CO2 and APO observations as tracers for anthropogenic emissions in both global and regional scale inversions and develop coupled land-atmosphere data assimilation in the global CO2MVS system constraining carbon cycle variables with satellite observations of soil moisture, LAI, SIF, and Biomass. This is addressed in a dedicated work package, WP3; *Improved use of in situ 14CO2 and APO observations to separate the impact of fossil fuel emissions from observed CO2 variability.* Within this WP, task T3.2 in CORSO is dedicated to the compilation of a database of 14CO2/APO flux estimates from bottom-up (process-based) approaches and models, complementing existing CO2 bottom-up flux databases, and to be used as a prior knowledge of the fluxes in the inversion frameworks in WP3 (task 3.3 and 3.4), which assess the potential of 14CO2 and APO observations. Finally, CORSO will provide specific recommendations for the topics above for the operational implementation of the CO2MVS within the Copernicus programme.

2.2. Scope of this deliverable

2.2.1. Objectives of this deliverable

Final version of the APO and 14CO2 bottom-up flux databases for CORSO WP3 with an exhaustive coverage of all types of fluxes including intermediate products.

2.2.2. Work performed in this deliverable

Under this deliverable, different tasks were conducted by the task partners. Terrestrial and oceanic isotopic disequilibrium fluxes and nuclear emission datasets were prepared by Lund University and LSCE. Global and regional ocean flux databases were developed by the University of Bristol. An improved regional anthropogenic APO inventory was created by TNO. Future scenarios maps of global APO are being produced for 2030 and 2050 based on SSP1 of IPCC AR6. The aim of these datasets is to support modelling in CORSO WP3 (task 3.3. and 3.4) (in particular the definition of prior estimates of the fluxes and isotopic signatures for the inversions, to be controlled or kept fixed in the inversion process).

2.2.3. Deviations and counter-measures

The deliverable report was due to be submitted for review on December 6th, however, it was postponed to December 20th to incorporate input for Task 3.2.d Future Scenarios. The final results in the form of gridded data for said task will be available after January 2025.

2.3. Task partners:

Partners	
NEDERLANDSE ORGANISATIE VOOR TOEGEPAST NATUURWETENSCHAPPELIJK ONDERZOEK TNO	TNO
LUNDS UNIVERSITET	ULUND
UNIVERSITE PAUL SABATIER TOULOUSE III	UT3-CNRS
UNIVERSITY OF BRISTOL	UNIVBRIS
COMMISSARIAT À L' ENERGIE ATOMIQUE ET AUX ENERGIES ALTERNATIVES	CEA

3. $\Delta^{14}CO_2$

3.1. Description of flux databases

Products are updated and improved compared to the datasets earlier provided as CORSO milestone MS6 and made available to project partners for a range of radiocarbon variables that are required for using radiocarbon observations in the inverse modelling systems in tasks 3.3 (global scale modelling) and 3.4 (regional scale modelling). These products include the isotopic disequilibrium fluxes, both terrestrial and oceanic, as well as the emissions from nuclear facilities, and are detailed below. Cosmogenic production fluxes are not updated since these can be calculated directly in the inversion systems following the approach by Wang (2016).

Oceanic disequilibrium fluxes

The ocean disequilibrium was split into its ocean-to-atmosphere and atmosphere-to-ocean components, with the ocean-to-atmosphere component of the data generated using the methodology found in Wang, 2016.

Briefly, the surface sea water content of ^{14}C was measured by the Global Ocean Data Analysis Project (GLODAP) and the ocean survey from Climate and Ocean: Variability, Predictability, and Change (CLIVAR); these two datasets have been conjoined into a gridded time series using the method outlined in Lindsay (2016). The GLODAP dataset provides a gridded map of $\Delta^{14}C$ in the ocean for the year 1995, based on samples of $\Delta^{14}C$ in sea surface water from samples collected during the 1970s and 1990s (Key, 2004). These maps were then extended by a decade using the CLIVAR survey, which provides transect measurements of $\Delta^{14}C$ in sea surface water between 2000-2011. The rate of change at each CLIVAR cruise location over time (units of ‰ yr^{-1}) was determined for a range of latitudes in each ocean basin using latitude-based spline functions (Figure 3.1). These spline functions were then applied to the gridded 1995 GLODAP map to generate ocean isotopic signatures for the 2004-2024 time period. The gridded maps of $\Delta^{14}C$ have been converted to $\delta^{14}C$ using an ocean-atmosphere fractionation coefficient, which is assumed to be twice the value of the ocean-atmosphere fractionation coefficient of $\delta^{13}C$ as given by the temperature-dependent empirical function in Tans et al. (1993).

The final data for CORSO are provided in the form of a gridded map of the ocean-to-atmosphere at a resolution of 2.5° latitude x 3.75° longitude for the year 2004 (Figure 3.2). The CLIVAR extrapolations indicate a variable rate of change for $\delta^{14}C$ over time that varies between -5.5 and 3.0 ‰ yr^{-1} depending on latitude and longitude. These rates have also been provided for each 2.5° latitude x 3.75° longitude grid cell.

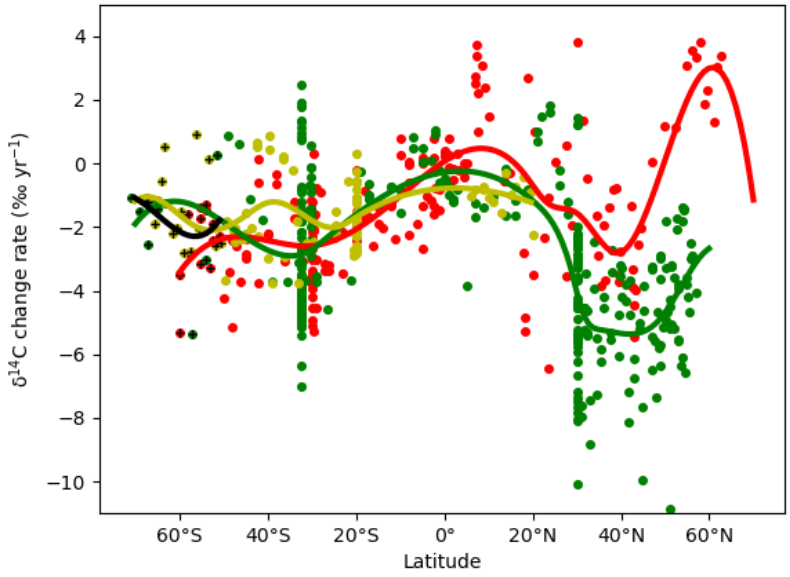

Figure 3.1. Rate of change for δ14C across different latitudes based on data from the CLIVAR cruises. The observations from the Atlantic Ocean (red), Pacific Ocean (green), Indian Ocean (yellow), and Southern Ocean (black marks) are fitted using smoothing splines.

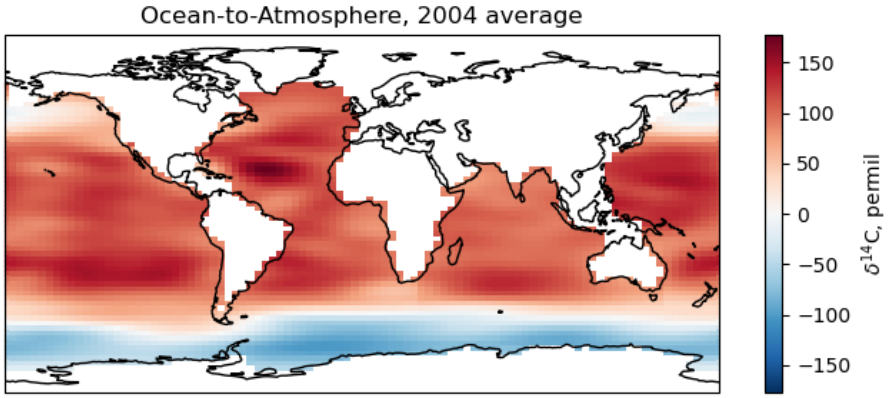

Figure 3.2. The 2004 average of the ocean-to-atmosphere δ14C isotopic signature.

Terrestrial disequilibrium fluxes

Simulations have been performed with the carbon isotope enabled dynamic global vegetation model LPJ to estimate the terrestrial disequilibrium flux for the recent historical period. A detailed description of the LPJ model is provided by Sitch et al. (2003) and of the isotope-enabled version by Scholze et al. (2003). In brief, LPJ operates on a gridcell basis and simulates average individual plant functional types (PFT) in a given gridcell. To calculate gridcell wide terrestrial carbon fluxes and pools the average individual PFT values are upscaled by the number of individuals per gridcell. The enhanced version of LPJ used here fully incorporates C isotopes as a tracer in the carbon cycle simulated by the model. The carbon isotope module includes the calculation of isotope fractionation during photosynthesis following the approach of Lloyd and Farquhar (1994), and separate accounting of all internal carbon pools for total C and ^{14}C. Photosynthesis and carbon isotope discrimination are calculated on a daily time step representing daily average values; assimilated CO_2 and $^{14}CO_2$ are allocated to the four different tissue pools (leaves, sap- and heart-wood, roots) on an

annual basis. Soil and litter total C and ^{14}C pools are updated monthly. As isotope fractionation processes during respiration are poorly understood, no fractionation is assigned for the decomposition.

LPJ requires meteorological input data (temperature, precipitation and incoming solar radiation), which here are taken from the monthly high-resolution gridded multivariate CRU TS v4.07 climate dataset (Harris et al., 2020). Besides the climate data the isotope-enabled version of LPJ requires atmospheric global CO_2 and hemispheric $\Delta^{14}CO_2$ content as additional input. Time-series of atmospheric CO_2 have been taken from McGuire et al. (2001) and extended until 2022 using data from NOAA's global monitoring programme (https://gml.noaa.gov/ccgg/trends/data.html). Atmospheric $\Delta^{14}CO_2$ content is taken from Graven et al. (2020).

The simulation has been performed at global scale with a 0.5º x 0.5º spatial and monthly temporal resolution for the years 1901 to 2022 following a 1000-year spin up period recycling the first 30 years of the climate input data (1901-1930). Output in the form of netcdf files has been made available for the years 1950 to 2022 for the gross CO_2 and $\Delta^{14}CO_2$ fluxes (NPP, Rhet and emissions from biomass burning, which are only available on an annual timescale) as well as for the terrestrial disequilibrium flux (ie. the terrestrial disequilibrium multiplied by the sum of heterotrophic respiration and 1/12 of the annual biomass burning emissions).

Figures 3.2 and 3.3 show the monthly averaged net ecosystem exchange as well we the terrestrial disequilibrium flux over Europe for the year 2010 as simulated by LPJ and compared to a simulation from ORCHIDEE and the posterior flux from Basu et al. (2020) (for NEE, Fig 3.2). All three simulations agree reasonably well on the timing of the seasonal fluxes (i.e. minimum and maximium of NEE), however LPJ shows a somewhat smaller seasonal amplitude than both ORCHIDDE and the posterior flux from from Basu et al. (2020). In the case of the terrestrial disequilibrium flux the LPJ simulation is compared only to the results from Basu et al. (2020) (Fig 3.3). There is a pronounced difference in both timing and amplitude of the seasonal cycle between the two estimates: the terrestrial disequilibrium flux from Basu et al. (2020) has its maximum value in September while LPJ shows a maximum terrestrial disequilibrium flux in July. The difference in the amplitude is even more pronounced with approximately 1.5 TgC $\Delta^{14}C$ d-1 from Basu et al. (2020) and only 0.5 TgC $\Delta^{14}C$ d-1 from LPJ. This illustrates the large uncertainty in the terrestrial isotopic disequilibrium.

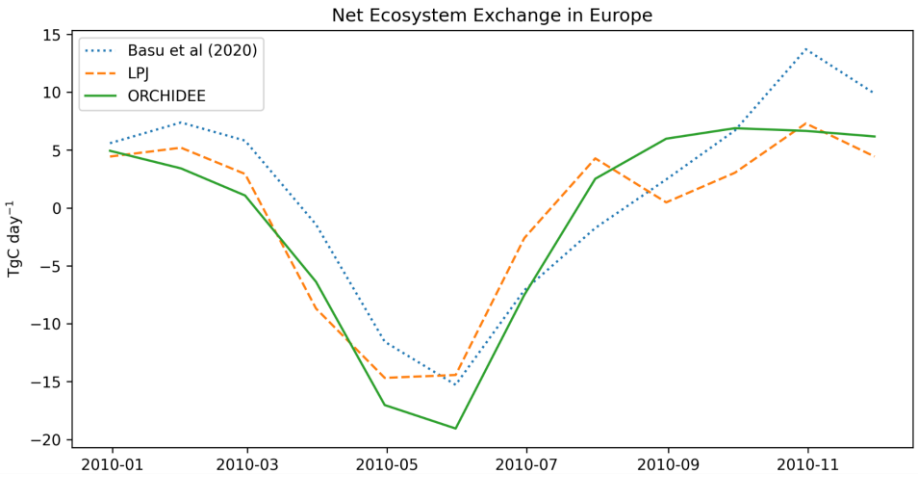

Figure 3.2. Comparison of monthly NEE as simulated by LPJ and ORCHIDEE as well as the optimised NEE from Basu et al. (2020) for the year 2010 and over Europe.

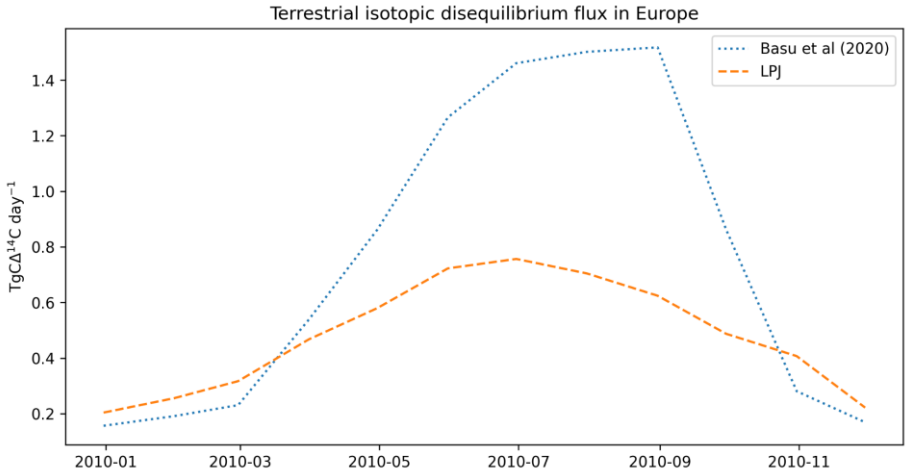

Figure 3.3. Comparison of the terrestrial isotopic disequilibrium flux as emulated by LPJ and from Basu et al. (2020) for the year 2010 and over Europe.

Figure 3.4 shows the spatial distribution of both the disequilibrium and the disequilibrium flux for a winter and a summer month (in 2022) as simulated by LPJ.

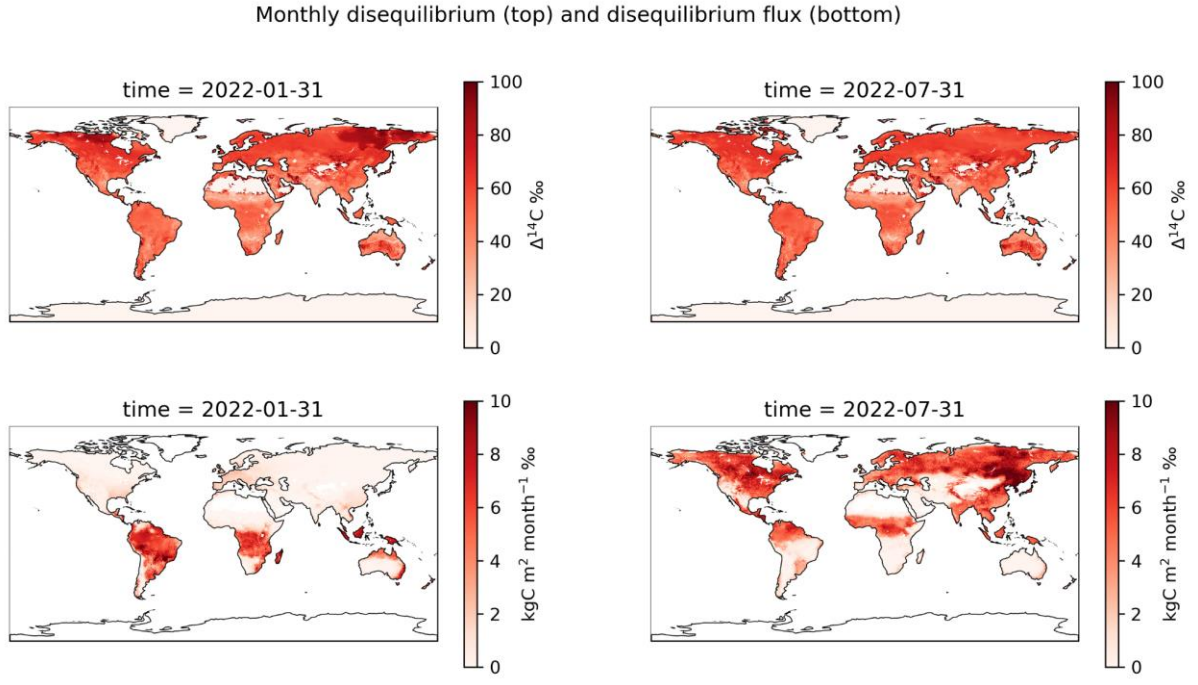

Figure 3.4 Terrestrial isotopic disequilibrium (top) and monthly terrestrial isotopic disequilibrium flux (bottom) as simulated by the isotope-enabled version of LPJ for a winter month (left) and a summer month (right) at 0.5 degree resolution.

Emissions from nuclear facilities

Emissions from nuclear power plants and spent fuel reprocessing plants have been produced based on the reported annual emissions from the European Commission Radioactive Discharges Database (RADD) as point sources. For nuclear facilities outside the European Union, we use the emission factors estimated by Graven and Gruber (2011) (https://doi.org/10.5194/acp-11-12339-2011) and Zazzeri et al. (2018)

(https://doi.org/10.1017/RDC.2018.42) and energy production data from the Power Reactor Information System (PRIS) (https://pris.iaea.org/PRIS/home.aspx). Emissions from other nuclear sites within the European domain have been obtained as explained in Appendix A.1. of Maier et al (2023). Emissions from the Spent Fuel Reprocessing Plant Tokai (Japan) were obtained from a report by the Japan Atomic Energy Agency (Nakada et al., 2008).

The data is available in two formats, one as point source data and one as gridded data (shown in Figures 3.5 for Europe and 3.6 for the globe). The gridded data has a horizontal resolution of 0.5ºx0.5º for Europe and 1ºx1º globally and a yearly temporal resolution in units of Bq m^-2 s^-1. The nuclear emissions can be calculated at different horizontal, temporal resolutions, or units using a dedicated Jupyter notebook. Figure 3.7 shows the annual emissions for the La Hague SFR plant over the time period 2006 to 2022.

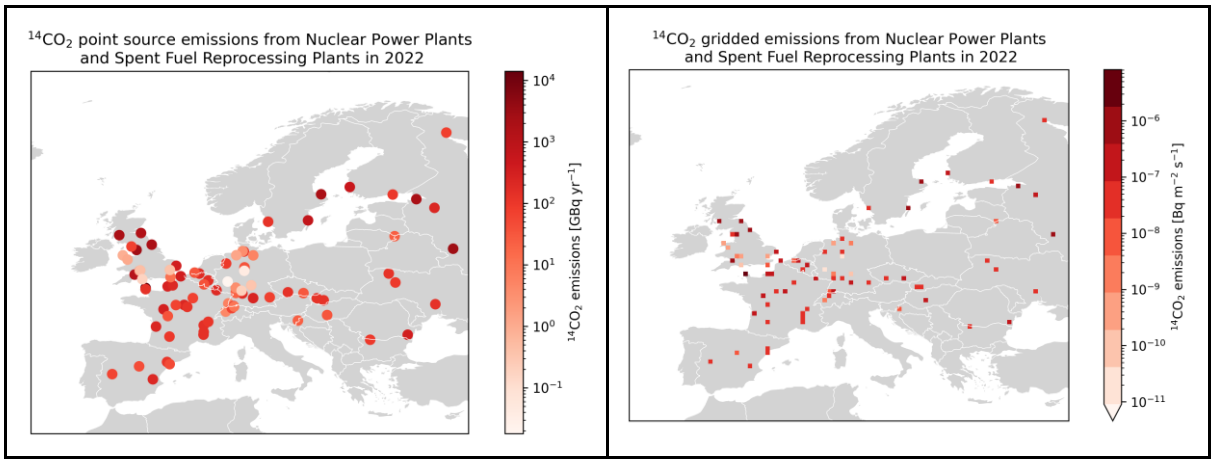

Figure 3.5. 14CO2 point source (left) and gridded (right) emissions from Nuclear Power Plants and Spent Fuel reprocessing Plants in Europe in 2022.

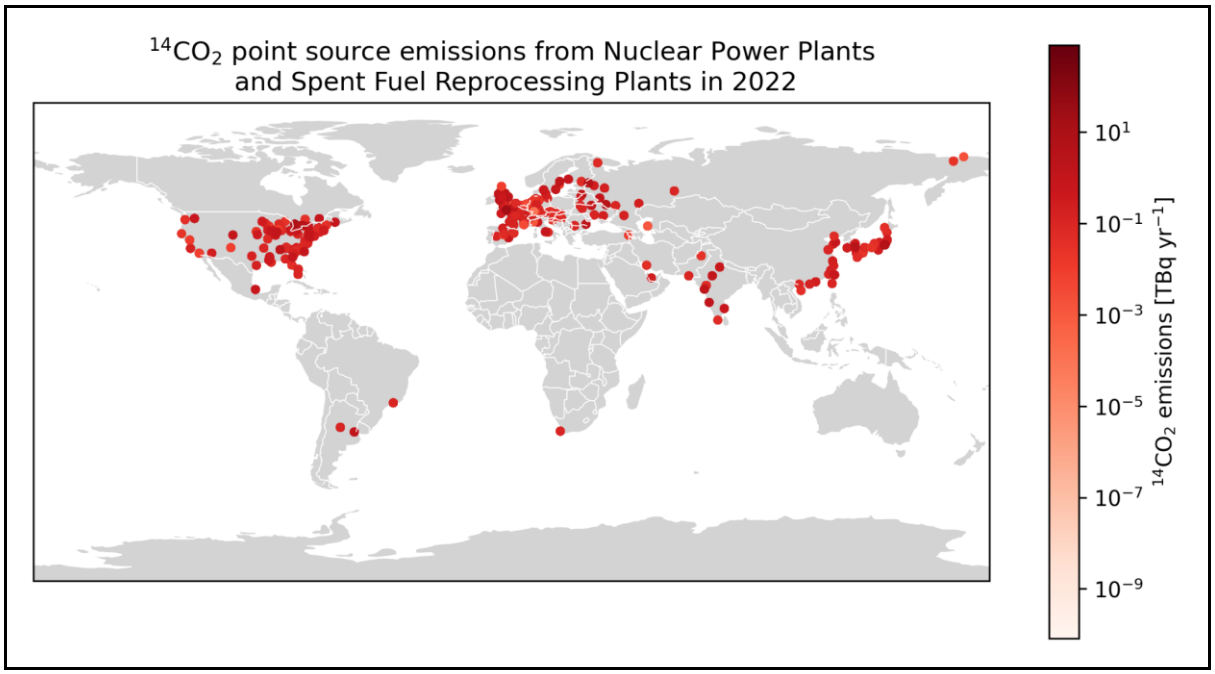

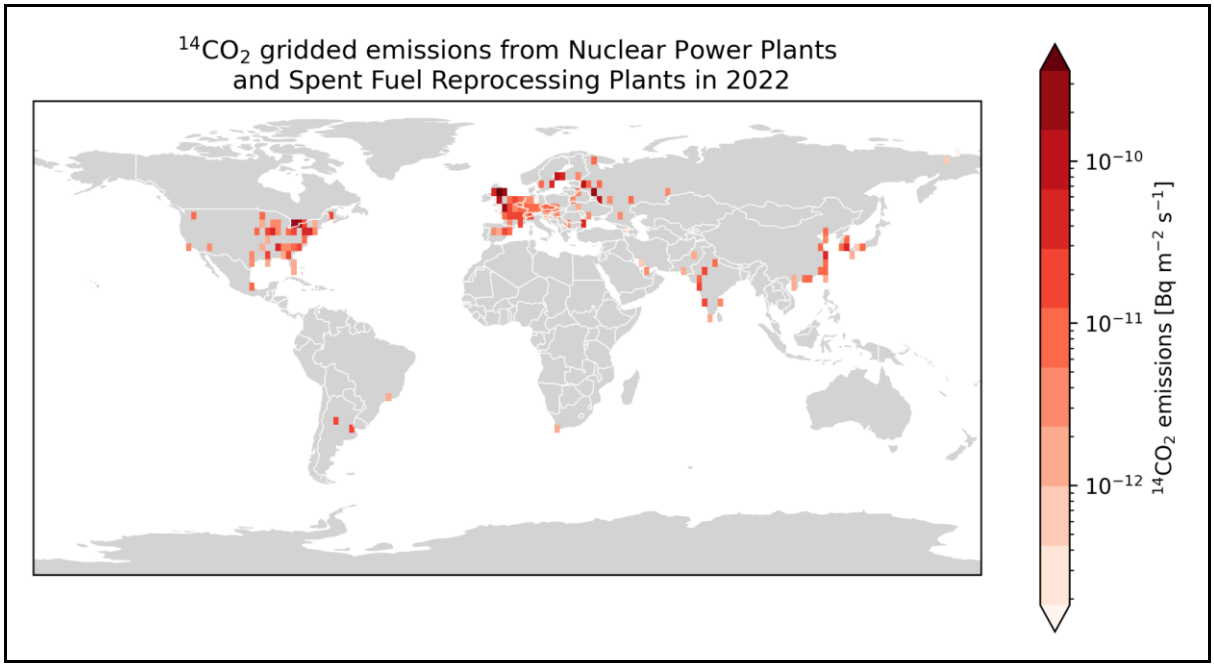

Figure 3.6. 14CO2 point source (top) and gridded (bottom) emissions from Nuclear Power Plants and Spent Fuel Reprocessing Plants in 2022.

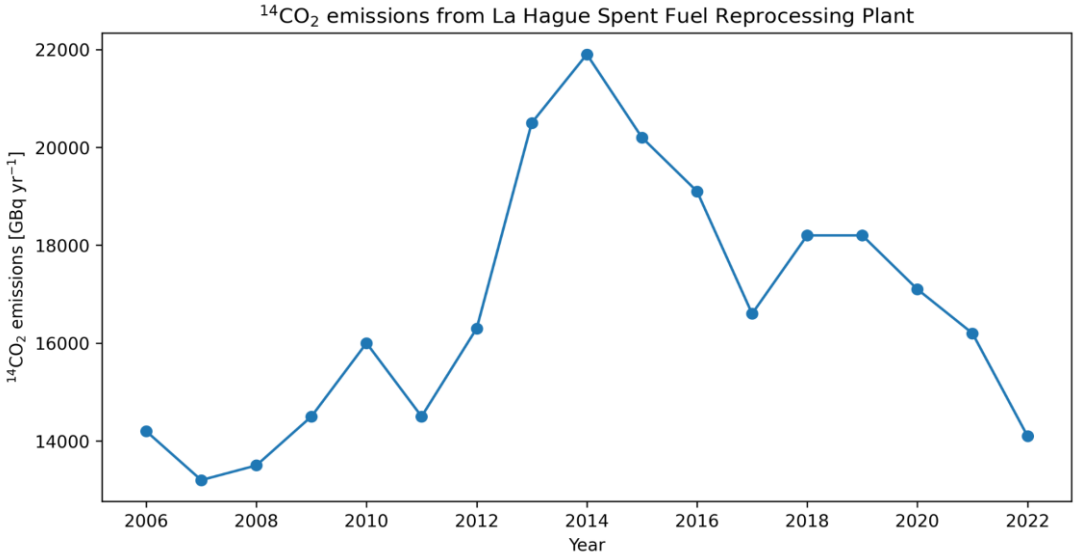

Figure 3.7. The figure shows the emission time series for the La Hague SFR plant.

3.2. Data availability

- The nuclear emissions and ocean disequilibrium data can be accessed through:

https://github.com/cdgomezo/corso-nuclear-emissions

- For the terrestrial fluxes, a more detailed description and accompanying papers are available on the CORSO project website and the data is available upon request by contacting Marko Scholze (marko.scholze@nateko.lu.se).
- The terrestrial data can be accessed through:

https://lu.box.com/s/0mxp9t7iu2ri1torlu2u7492zbur468n

CORSO

3.3. Contact Person(s)

Lund University

Carlos Gomez (carlos.gomez@nateko.lu.se)

Marko Scholze (marko.scholze@nateko.lu.se)

CEA (LSCE)

Hannah Allen (hannah.allen@lsce.ipsl.fr)

Grégoire Broquet (gregoire.broquet@lsce.ipsl.fr)

3.4. References

Basu, S., Miller, J. B., and Lehman, S.: Separation of biospheric and fossil fuel fluxes of CO2 by atmospheric inversion of CO2 and 14CO2 measurements: Observation System Simulations, Atmos. Chem. Phys., 16, 5665–5683, https://doi.org/10.5194/acp-16-5665-2016, 2016.

Graven, H. D. and Gruber, N.: Continental-scale enrichment of atmospheric 14CO2 from the nuclear power industry: potential impact on the estimation of fossil fuel-derived CO2, Atmos. Chem. Phys., 11, 12 339–12 349, https://doi.org/10.5194/acp-11-12339-2011, 2011.

Graven, H., Keeling, R. F., and Rogelj, J.: Changes to carbon isotopes in atmospheric CO_2 over the industrial era and into the future, Glob. Biogeochem. Cycles, 34, e2019GB006170, https://doi.org/10.1029/2019GB006170, 2020.

Harris, I., Osborn, T. J., and Jones, P.: Version 4 of the CRU TS monthly high-resolution gridded multivariate climate dataset, Sci. Data, 7, 109, https://doi.org/10.1038/s41597-020-0453-3, 2020.

Key, R. M., Kozyr, A., Sabine, C. L., Lee, K., Wanninkhof, R., Bullister, J. L., Feely, R. A., Millero, F. J., Mordy, C., and Peng, T.-H.: A global ocean carbon climatology: Results from Global Data Analysis Project (GLODAP), Glob. Biogeochem. Cycles, 18, GB4031, https://doi.org/10.1029/2004GB002247, 2004.

Lindsay, C. M.: Carbon dynamics of the deglacial and contemporary ocean inferred from radiocarbon measurements in foraminifera, seawater and atmospheric carbon dioxide. Ph.D. thesis. Geological Sciences, University of Colorado Boulder, 2016.

Maier, F., Levin, I., Gachkivskyi, M., Rödenbeck, C., and Hammer, S.: Estimating regional fossil fuel CO2 concentrations from 14CO2 observations: challenges and uncertainties, Philosophical Transactions of the Royal Society A, 381, https://doi.org/10.1098/RSTA.2022.0203, 2023.

Nakada, A., Miyauchi, T., Akiyama, K., Momose, T., Kozawa, T., Yokota, T. and Ohtomo, H.: Radioactive airborne effluent discharged from Tokai reprocessing plant. 1998-2007, Japan Atomic Energy Agency, Tokai, Ibaraki (Japan). [online] Available from: https://inis.iaea.org/search/search.aspx?orig_q=RN:40102398 (Accessed 3 December 2024), 2008.

Scholze, M., Kaplan, J. O., Knorr, W., and Heimann, M.: Climate and interannual variability of the atmosphere-biosphere $^{13}CO_2$ flux, Geophys. Res. Lett., 30, 1097, https://doi.org/10.1029/2002GL015631, 2003.

Sitch, S., Smith, B., Prentice, I. C., Arneth, A., Bondeau, A., Cramer, W., Kaplan, J. O., Levis, S., Lucht, W., Sykes, M. T., Thonicke, K., and Venevsky, S.: Evaluation of ecosystem dynamics, plant geography, and terrestrial carbon cycling in the LPJ dynamic global vegetation model, Glob. Change Biol., 9, 161–185, https://doi.org/10.1046/j.1365-2486.2003.00569.x, 2003.

Tans, P. P., Berry, J. A. and Keeling, R. F.: Oceanic 13C/12C observations: a new window on ocean CO2 uptake, Global Biogeochem. Cycles, 7(2), 353–368, 1993.

Wang, Y.: The potential of observations of radiocarbon in atmospheric CO_2 for the atmospheric inversion of fossil fuel CO_2 emission at regional scale, Ph.D. thesis, Earth Sci., Univ. Paris Saclay (CO-mUE), 2016.

Zazzeri, G., Acuña Yeomans, E., and Graven, H. D.: Global and Regional Emissions of Radiocarbon from Nuclear Power Plants from 1972 to 2016, Radiocarbon, 60, 1067–1081, https://doi.org/DOI: 10.1017/RDC.2018.42, 2018.

4. APO Oceans

Ocean flux databases do not typically provide air-sea fluxes of atmospheric potential oxygen (APO). Usually, APO fluxes must be calculated from the oxygen (O_2), carbon dioxide (CO_2), and nitrogen (N_2) flux fields (e.g. Manning and Keeling, 2006; Chawner et al., *preprint.*). Like other flux data products, ocean flux databases are compiled using different approaches. Flux databases, such as NEMO-ERSEM and ECCO-Darwin, are formed by combining an ocean circulation model with an ecosystem model to produce three-dimensional air-sea flux fields of various atmospheric species. Other flux data products, such as Jena-Carboscope, derive global air-sea flux estimates through Bayesian inference using atmospheric O_2 and CO_2 measurements from a global measurement network.

Some of the CORSO WP3 objectives require both global and regional scale (over Europe) APO flux products. Below we describe the flux products we intend to use for the modelling work associated with WP3.

4.1. Description of global flux databases

Fluxes from three databases will be used to form global APO flux estimates. These databases correspond to some of those being used in a forward-model APO intercomparison project being led by Britt Stephens and Matt Long from NCAR that are relevant to global oceanic fluxes.

Jena Carboscope (Rödenbeck et al., 2008) produces APO and CO2 fluxes based on top-down posterior emissions derived from a global inversion using atmospheric measurements from 23 CO2 stations and 10 O2 stations that are part of the Scripps Institute of Oceanography network and are based in remote locations. CO2 fluxes are estimated from the interpolation of pCO2 data.

The Seasonal-to-Multiyear Large Ensemble (SMYLE; Yeager et al., 2022) uses CESM2 (Community Earth System Model v2; Danabasoglu et al., 2022) for exploring near-term predictability of all Earth system components represented in CESM2. The CESM2 has a forced-ocean-sea-ice (FOSI) configuration for obtaining ocean and sea ice model parameters of air-sea O2, CO2, and N2 fluxes from JRA55-do (Tsujino et al., 2018) forced ocean-ice integration over 1958-2020.

The third database consists of bottom-up air-sea flux estimates of O2, CO2, and N2. Oxygen flux fields are constructed using the seasonal component of dissolved O2 measurement-based climatology of Garcia and Keeling (2001) scaled by a factor of 0.82 (Naegler et al., 2006) and with the annual mean component take from an ocean inversion (Resplandey et al., 2016). Carbon dioxide flux fields are taken from the pCO2 product of Landschützer et al. (2016) and N2 fluxes are estimated from the ERA5 heat fluxes and sea-surface temperature data.

4.2. Description of regional flux databases

NEMO-ERSEM (Nucleus for European Modeling of the Ocean – European Regional Seas Ecosystem Model) is a modelling framework that produces high-resolution flux outputs for the European Continental Shelf. NEMO is a widely used, open-source ocean model that simulates the physical processes of the ocean (Madec, 2008). ERSEM is a biogeochemical model used for simulating the interactions between different components of marine ecosystems (Butenschön et al., 2016). The NEMO-ERSEM dataset is based on the Atlantic Margin Model 7 km NEMO configuration. It extends over the northwest European shelf and northeast Atlantic Ocean (ECMWF Confluence). Components of NEMO-ERSEM, such as the model nutrient

fields, have previously been validated against other regional ocean models often finding NEMO-ERSEM performs well (Edwards et al. 2012).

ECCO-Darwin is a global ocean biogeochemistry model that uses data assimilation from both physical and biogeochemical observations (Carroll et al., 2020). The model consists of an adjoint-based ocean circulation estimate (ECCO) and an ecosystem model (Darwin). ECCO-Darwin determines ocean-atmosphere transfer of O_2 and CO_2 by combining the partial pressure differences across the air-sea interface with the relationship between wind speed and gas transfer, as described by Wanninkhof (1992). The Darwin Project biogeochemical model resolves the cycling of CO_2 and O_2 and its ocean ecology includes phytoplankton and zooplankton (Brix et al., 2015; Carroll et al., 2020).

4.3. Data availability

Jena Carboscope: Daily APO and CO_2 flux fields with 2.0^ox2.5^o horizontal resolution spanning globally with temporal coverage from 1999-2020. Data files that include/exclude atmospheric measurements from Weybourne atmospheric observatory are available. Original data files available from Jena Carboscope:

http://www.bgc-jena.mpg.de/CarboScope/?ID=apo

Filename:

SFAPO_OCN.carboscope.apo99X_v2021.1x1.19860101-20201231.nc

CESM2-FOSI: Daily CO_2 and O_2 output fluxes and monthly heat flux data used for deriving N_2 fluxes. Spatial resolution of 1.0^ox1.0^o with global coverage and temporal span covering 1958-2020. Data files available from:
https://app.globus.org/file-manager?origin_id=7e5b68e0-941e-11ec-bad4-cd8db799a66a&origin_path=%2F

Filenames:

SFO2_OCN.cesm_fosi_smyle.1x1.19860101-20201231.nc
SFCO2_OCN.cesm_fosi_smyle.1x1.19860101-20201231.nc
SFN2_OCN.cesm_fosi_smyle.1x1.19860101-20201231.nc

Bottom-Up fluxes: Oxygen fluxes from Garcia and Keeling (2001) have monthly timesteps covering 1986-2020 with spatial resolution of 1.125^ox1.125^o. Annual oxygen fluxes from Resplandey et al. (2016) are available over 21 regions across the globe available over 1986-2020. Carbon dioxide fluxes spanning 1982-2020 with monthly time resolution and 1.0^ox1.0^o spatial resolution with global coverage. Nitrogen fluxes are derived from ERA5 heat fluxes which span 1979-2021 with monthly time resolution and 0.25^ox0.25^o spatial resolution. Data files available from:
https://app.globus.org/file-manager?origin_id=7e5b68e0-941e-11ec-bad4-cd8db799a66a&origin_path=%2F

Filenames:

SFO2_OCN.gk2001_R2016.1x1.repeat_monclim.19860101-20201231.nc
SFCO2_OCN.MPI-SOM-FFN.1x1.19860101-20201231.nc
SFN2_OCN.era5_shf.1x1.19860101-20201231.nc

CORSO

NEMO-ERSEM (v1.7): Daily and monthly flux fields with 0.06ºx0.06º horizontal resolution, 43 vertical layers covering the Northwest European Shelf (20W to 13E, 40N to 65N). With temporal coverage from January 2006 to December 2049. Data available through The Climate Data Store:

https://cds.climate.copernicus.eu/cdsapp#!/dataset/sis-marine-properties?tab=overview

ECCO-Darwin: Daily flux fields with 1/3^{O} spatial resolution at the equator and ~18 km at high latitudes, 50 vertical layers and temporal coverage spanning 1992-2019. Global fields are available but split between 17 biomes, with biomes 3 relating to the North Sea. Data are available on Zenodo: https://zenodo.org/record/3829965

4.4. Contact Person(s)

University of Bristol

Eric Saboya (eric.saboya@bristol.ac.uk)

4.5. References

Butenschön, M., Clark, J., Aldridge, J. N., Allen, J. I., Artioli, Y., Blackford, J., Bruggeman, J., Cazenave, P., Ciavatta, S., Kay, S., Lessin, G., van Leeuwen, S., van der Molen, J., de Mora, L., Polimene, L., Sailley, S., Stephens, N., and Torres, R.: ERSEM 15.06: a generic model for marine biogeochemistry and the ecosystem dynamics of the lower trophic levels, Geosci. Model Dev., 9, 1293–1339, https://doi.org/10.5194/gmd-9-1293-2016, 2016.

Brix, H., Menemenlis, D., Hill, C., Dutkiewicz, S., Jahn, O., Wang, D., Bowman, K., and Zhang, H.: Using Green's Functions to initialize and adjust a global, eddying ocean biogeochemistry general circulation model, Ocean Modelling, 95, 1–14, https://doi.org/https://doi.org/10.1016/j.ocemod.2015.07.008, 2015.

Carroll, D., Menemenlis, D., Adkins, J. F., Bowman, K. W., Brix, H., Dutkiewicz, S., et al.: The ECCO-Darwin data-assimilative global ocean biogeochemistry model: Estimates of seasonal to multidecadal surface ocean pCO_2 and air-sea CO_2 flux, J. Adv. Model. Earth Syst., 12, e2019MS001888, https://doi.org/10.1029/2019MS001888, 2020.

Chawner, H., Adcock, K. E., Arnold, T., Artioli, Y., Dylag, C., Forster, G. L., Ganesan, A., Graven, H., Lessin, G., Levy, P., Luijx, I. T., Manning, A., Pickers, P. A., Rennick, C., Rödenbeck, C., and Rigby, M.: Atmospheric oxygen as a tracer for fossil fuel carbon dioxide: a sensitivity study in the UK, EGUsphere [preprint], https://doi.org/10.5194/egusphere-2023-385, 2023.

Danabasoglu, G., Deser, C., Rodgers, K., and Timmermann, A.: The CESM2 Large Ensemble Dataset, Climate Data Gateway at NCAR [data set], https://doi.org/10.26024/kgmp-c556, 2022.

ECMWF Confluence. https://confluence.ecmwf.int/pages/viewpage.action?pageId=283550184. Accessed October 10, 2023.

Edwards, K. P., Barciela, R., and Butenschön, M.: Validation of the NEMO-ERSEM operational ecosystem model for the North West European Continental Shelf, Ocean Sci., 8, 983–1000, https://doi.org/10.5194/os-8-983-2012, 2012.

Garcia, H. E. and Keeling, R. F.: On the global oxygen anomaly and air-sea flux, J. Geophys. Res. C: Oceans, 106, 31155–31166, 2001.

Landschützer, P., Gruber, N., and Bakker, D. C. E.: Decadal variations and trends of the global ocean carbon sink, Global Biogeochem. Cycles, 30, 1396–1417, https://doi.org/10.1002/2015gb005359, 2016.

Madec, G.: NEMO ocean engine, Note du Pôle de Modélisation, 27, Institut Pierre-Simon Laplace (IPSL), France, 300 pp., 2008.

Manning, A. C. and Keeling, R. F.: Global oceanic and land biotic carbon sinks from the Scripps atmospheric oxygen flask sampling network, Tellus B, 58, 95–116, https://doi.org/10.1111/j.1600-0889.2006.00175.x, 2006.

Naegler, T., Ciais, P., Rodgers, K., and Levin, I.: Excess radiocarbon constraints on air-sea gas exchange and the uptake of CO_2 by the oceans, Geophys. Res. Lett., 33, https://doi.org/10.1029/2005gl025408, 2006.

Resplandy, L., Keeling, R. F., Stephens, B. B., Bent, J. D., Jacobson, A., Rödenbeck, C., and Khatiwala, S.: Constraints on oceanic meridional heat transport from combined measurements of oxygen and carbon, Clim. Dyn., 47, 3335–3357, https://doi.org/10.1007/s00382-016-3029-3, 2016.

Rödenbeck, C., Le Quéré, C., Heimann, M., and Keeling, R. F.: Interannual variability in oceanic biogeochemical processes inferred by inversion of atmospheric O_2/N_2 and CO_2 data, Tellus B, 60, 685–705, https://doi.org/10.1111/j.1600-0889.2008.00375.x, 2008.

Tsujino, H., Urakawa, S., Nakano, H., Small, R. J., Kim, W. M., Yeager, S. G., Danabasoglu, G., Suzuki, T., Bamber, J. L., Bentsen, M., Böning, C. W., Bozec, A., Chassignet, E. P., Curchitser, E., Dias, F. B., Durack, P. J., Griffies, S. M., Harada, Y., Ilicak, M., Josey, S. A., Kobayashi, C., Kobayashi, S., Komuro, Y., Large, W. G., Le Sommer, J., Marsland, S. J., Masina, S., Scheinert, M., Tomita, H., Valdivieso, M., and Yamazaki, D.: JRA-55 based surface dataset for driving ocean–sea-ice models (JRA55-do), Ocean Model., 130, 79–139, https://doi.org/10.1016/j.ocemod.2018.07.002, 2018.

Wanninkhof, R.: Relationship between wind speed and gas exchange over the ocean, Journal of Geophysical Research: Oceans, 97, 7373– 7382, https://doi.org/https://doi.org/10.1029/92JC00188, 1992.

Yeager, S. G., Rosenbloom, N., Glanville, A. A., Wu, X., Simpson, I., Li, H., Molina, M. J., Krumhardt, K., Mogen, S., Lindsay, K., Lombardozzi, D., Wieder, W., Kim, W. M., Richter, J. H., Long, M., Danabasoglu, G., Bailey, D., Holland, M., Lovenduski, N., Strand, W. G., and King, T.: The Seasonal-to-Multiyear Large Ensemble (SMYLE) prediction system using the Community Earth System Model version 2, Geosci. Model Dev., 15, 6451–6493, https://doi.org/10.5194/gmd-15-6451-2022, 2022.

5. APO anthropogenic Global

5.1. Description of flux databases

5.1.1. Describing the GridFED dataset

The GridFED dataset, full name GCP-GridFED, is a gridded fossil CO2 emissions and related O2 uptake database. Published in 2021 by Jones et al., the first version of GridFED was a global inventory with a spatial resolution of 0.1° x 0.1° and covered the period from 1959 to 2018. Updates are made at least annually. The latest version of the dataset provides monthly emissions of CO2 for the period 1959-2023, consistent with national emissions reported by the Global Carbon Project, due to coal, oil, and natural gas, and their use for mixed bunker fuels and the calcination of limestone during cement processes. The database was built by scaling monthly gridded emissions for 2010 from the Emissions Database for Global Atmospheric Research (EDGAR v4.3.2) to the national annual CO2 emissions based on the Global Carbon Budget (GCB-NAE) for the years 1959-2023. These estimates are based on country submissions to the United Nations Framework Convention on Climate Change (UNFCCC), and other sources for certain countries and older years, such as the Carbon Dioxide Information Analysis Centre (CDIAC) and based on energy statistics from the United Nations (UN). For recent years, emissions are estimated based on the annual BP Statistical Review of World Energy. The O2 uptake, defined by Equation 6.1, is calculated based on individual oxidative ratios (OR) for oil, coal and natural gas, and the OR for bunker oil is considered to be the same as that for oil. The data is shared as a NetCDF file under a Creative Commons License (Jones et al. (2021)).

5.2. Data availability

GCP-GridFED (version 2024.0) is a gridded fossil emissions dataset that is consistent with the national CO2 emissions reported by the Global Carbon Project (GCP). GCP-GridFEDv2024.0 provides monthly fossil CO2 emissions for the period 1959-2023 at a spatial resolution of 0.1° × 0.1°. GCP-GridFED also includes gridded uncertainties in CO2 emission, incorporating differences in uncertainty across emissions sectors and countries, and gridded estimates of corresponding O2 uptake based on oxidative ratios for oil, coal and natural gas. Data and description available from:

Gridded fossil CO2 emissions and related O2 combustion consistent with national inventories 1959-2023 | Zenodo

5.3. References

Jones, M. W., Andrew, R. M., Peters, G. P., et al.: Gridded fossil CO_2 emissions and related O_2 combustion consistent with national inventories 1959–2018, Sci. Data, 8, 2, https://doi.org/10.1038/s41597-020-00779-6, 2021.

6. APO anthropogenic Regional

6.1. Description of flux databases

6.1.1. Building a time series based on the existing APO inventory

The regional atmospheric potential oxygen (APO) inventory is based on earlier work started under the CHE project (https://www.che-project.eu/) for one single year (2015) based on the TNO-GHGco inventory in combination with the approach taken for the COFFEE data set (Steinbach et al., 2011). A brief description was given in the CHE deliverable 4.3 (CHE-D4-3-V4-1.pdf (che-project.eu)) and application was discussed in CHE Deliverable 4.4 (D4.4 Sampling Strategy for additional tracers | CO2 Human Emissions (che-project.eu). The European regional CO2 and co-emitted species emissions as used for the TNO regional APO product in CORSO are based on the emissions dataset produced by TNO for CAMS as described in Kuenen et al. (2022) for the period 2005-2023. Since the CAMS data for 2022 and 2023 is not yet available, forecasted emissions for these years were used for the EU27, the UK, and European Free Trade Association (EFTA) countries. For other countries within the domain, where forecasted data is unavailable, the 2021 emission values were used as estimates for 2022 and 2023.The latest version of the product is described in Denier van der Gon et al. (2023). The shipping emissions for the European domain are produced by the Finnish Meteorological Institute (FMI) using the Ship Traffic Emission Assessment Model (STEAM, Johansson et al., 2017; Jalkanen et al., 2016), which uses Automatic Identification System (AIS) data to describe ship traffic activity. Since data for 2023 was unavailable, the fuel splits from 2022 were used to fill the gap in the data. The most recent version of the data is documented in chapter 4 of Denier van der Gon et al. (2023).

O2 uptake is calculated by multiplying anthropogenic CO_2 emissions by an oxidative ratio (OR), defined as the molar ratio of oxygen (O_2) consumed to carbon dioxide (CO_2) produced during the combustion of organic material. The following equation is applied:

$$O_2\,(g) = \frac{OR \times MWO_2\,(g.mol^{-1}) \times CO_2(g)}{MWCO_2\,(g.mol^{-1})} \quad \text{[EQ 6.1]}$$

with MW referring to molecular weight

Current ORs are available for 5 main fuel types (i.e., solid, liquid, gas, biomass and waste) with specific ORs for different liquid transport fuels and stationary vs. mobile biomass. These ORs have either been based on values reported by Steinbach et al. (2011) or calculated by TNO using ultimate analysis data, which involves determining the elemental composition (e.g., carbon, hydrogen, nitrogen, sulphur, and oxygen) of these fuels, and applying the following function:

$$OR_{fuel} = 1 + 0.375 \times \frac{(8 \times f_H - f_O)}{f_C} \quad \text{[EQ 6.2]}$$

with f referring to the weight fractions of Hydrogen (H), Carbon (C) and Oxygen (O)

These ORs have been integrated into the CAMS timeseries emissions based on the fuel type. For sector-fuel combinations with no associated fuel type, no ORs could be introduced and thus no O2 uptake from CO2 could be calculated. Similarly, when CO2 emissions are null, such as the case of processes with no combustion, no OR is calculated.

There are two versions of the TNO gridded APO time series. APO-v2_0 was prepared for the CORSO milestone M6 and covers 2005-2020. APO_v3_0 is the updated product described in this deliverable report and covers the period 2005-2023. See section 6.2 for data availability.

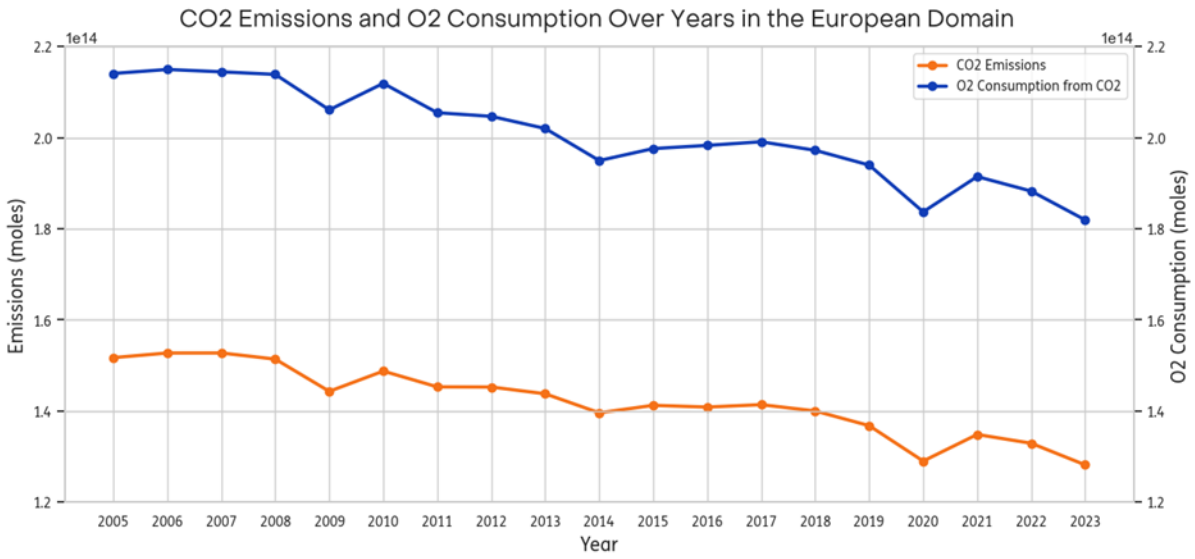

Figure 6.1: CO_2 emissions (left Y-axis) and O_2 uptake (right Y-axis) in moles

The timeseries is presented in kilotons, as users of this dataset require the mass quantities of emissions and O_2 consumption for their models. However, it is helpful to look at the values in terms of moles, to better observe the ORs applied between O_2 and CO_2 (see Figure 6.1).

6.1.2. Introducing improvements to the existing APO inventory

This current regional APO inventory has focused solely on the O_2 consumed by the formation of CO_2. With this simple method there is quite some room for improvement. Given the scope and time allocated for this project, the following suggested improvements were prioritised and executed:

O_2 uptake from the production of NOx, CO and SOx

Expanding on the previous definition of OR, the improved regional APO inventory includes O_2 uptake not only from CO_2 emissions, but also the emission of the following co-emitted species: NOx, CO and SOx. These emissions are based on the CAMS data and are represented in Figure 6.2. Note that NOx, CO and SOx are expressed in kton/yr but CO_2 emissions are divided by 1000 (effectively in Mton/yr). For the first two pollutants, the process is straight-forward, following the same equation (EQ 6.1) used for CO_2. This was applied for each sector-fuel combination for each country between 2005 and 2020. For SOx, the process is a little more complicated, as the presence of desulfurization units greatly reduces SOx emissions. For that reason, a correction factor was applied to account for the 90% removal efficiency of desulfurization units in the power sector.

Figure 6.2 also nicely illustrates the impact of air quality measures and improved technologies: the emissions of NOx, CO and SOx show a much steeper decline than CO_2 over the period 2005-2023. This implies that the impact of the co-emitted species on APO is also declining over time.

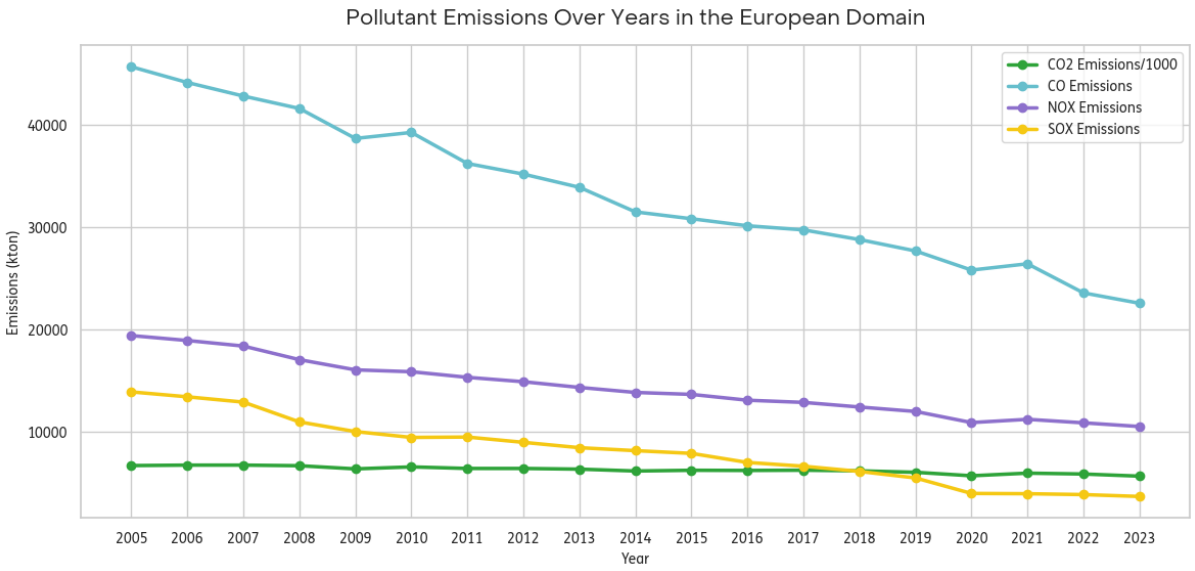

Figure 6.2: CO_2 and co-emitted species emissions based on CAMS data. CO_2 emissions were divided by a 1000 to better observe the change in different emissions across time.

As can be observed in Figure 6.3, taking into account co-emitted species has led to a slight increase in the amount of O_2 consumed. This marginal increase is attributed to two primary factors: firstly, these species have much lower emissions compared to CO_2, and secondly, they exhibit lower molar ratios for pollutants such as CO (½), NOx, and SOx (1), indicating the amount of O_2 required for their production. Furthermore, a decrease in this difference over time is also observed, due to the faster reduction in air pollutants compared to CO_2, as illustrated in Figure 6.2.

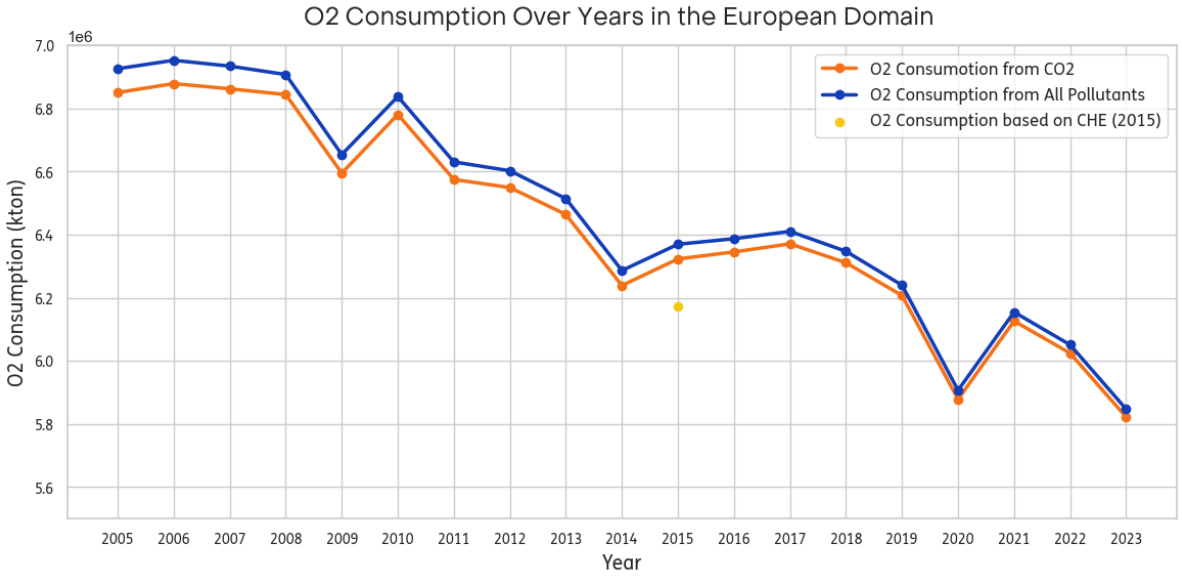

Figure 6.3: Comparison between O_2 uptake based on CO_2 and O_2 based on both CO_2 and the co-emitted species (CO, NOx, SOx), compared to the result from the CHE project (2015).

Refining ORs for sea shipping

Initially, one OR was introduced for all sea shipping fuels. It was generalised as an OR of 1.44, for any liquid fuel. However, given the diversity in international sea shipping fuel, there was

some room for a more detailed approach. Based on data provided by the FMI regarding the proportion of fuel-type used between 2005-2023 in different seas, three main types of fuels were identified:

1. Liquified Natural Gas (LNG) with an OR of gas fuel of 1.95 (Steinbach et al., 2011)
2. Heavy Fuel Oil (HFO) with an OR of 1.35 (TNO, 2019)
3. Marine Oils, i.e., Marine Gas Oil (MGO) and Marine Diesel Oil (MDO) with an OR of 1.46, calculated based on ultimate analysis data and using EQ 6.2.

As illustrated in Figure 6.4, the O_2 consumption calculated using the fixed OR of 1.44 was consistently higher than the refined estimates, both with and without accounting for co-emitted species. However, from 2020 onward, the refined ORs result in higher O_2 consumption. This shift is attributed to the growing share of LNG in the sea shipping fuel mix, which has an OR of 1.95—substantially higher than the ORs for traditional fuels like HFO and MDO/MGO, which are closer to the fixed value of 1.44. Between 2005 and 2022, the share of LNG increased nearly 8.5-fold and is expected to continue rising as the industry transitions to cleaner shipping fuels.

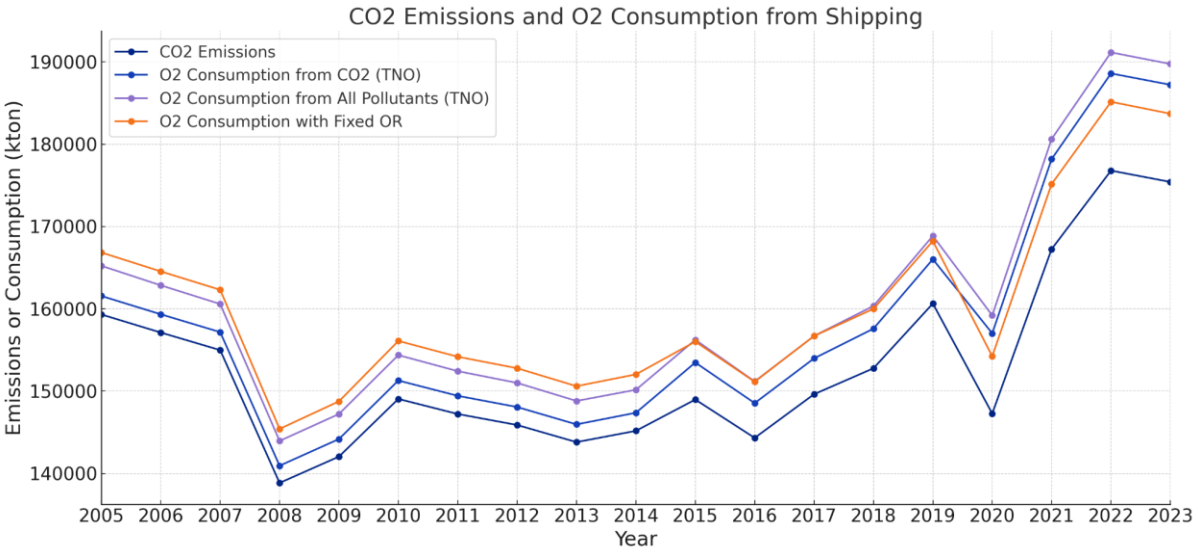

Figure 6.4: Comparison between the O_2 consumed with the refined (TNO APO Inventory) and the fixed sea shipping ORs (as used by Steinbach et al., 2011)

This highlights the growing importance of refining ORs to ensure accurate assessments of O_2 consumption in the future, particularly as sea shipping, though smaller in scale compared to other fuel sources, still exerts a significant impact on the inventory. Figure 6.5 shows the relative importance of sea shipping on the O2 consumption

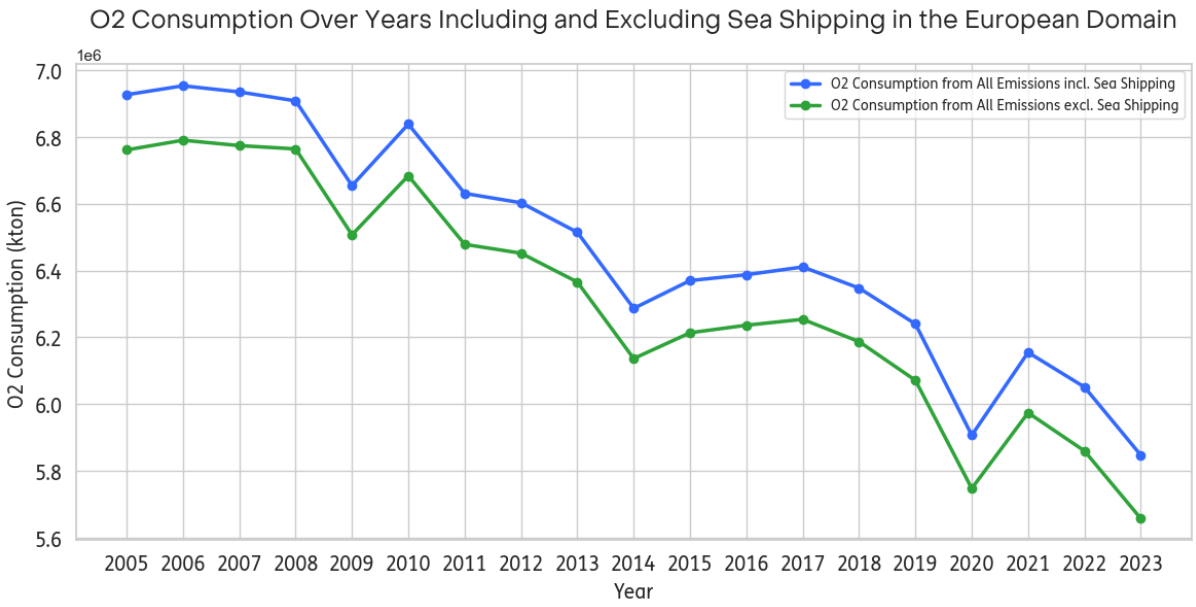

Figure 6.5: Comparison between the O_2 consumed with and without including emissions from international sea shipping.

To provide a clearer visualization of the inventory, Figure 6.6 displays the gridded emission data spatially distributed across the European domain for 2023. Notably, urban centers, including major cities like Paris, London, and Madrid, as well as industrial hubs around Antwerp, Rotterdam, and Düsseldorf, stand out with high O_2 consumption. In contrast, shipping routes are also discernible, though they exhibit comparatively lower O_2 consumption. Compared to MS6, which only covered the EU27, the domain has been extended, especially to the east.

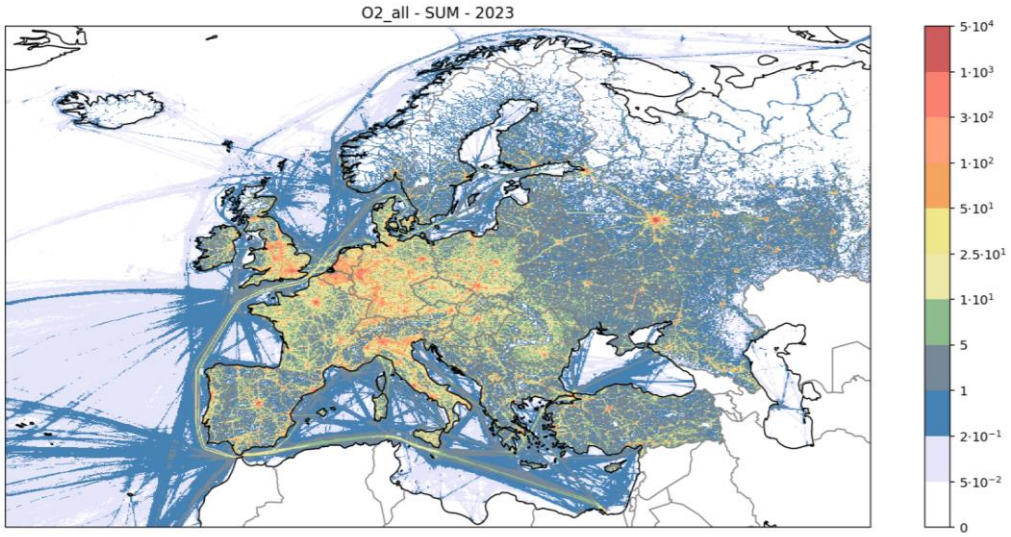

Figure 6.6: Total O_2 consumption (kton/gridcell) from fuel combustion in 2023.

CORSO

6.1.3. Comparison to global APO inventories

The data from the regional APO inventory is being compared to the CHE product for 2015 and two global datasets:

- CHE
- GridFED
- COFFEE

CHE

Comparison with the TNO APO inventory for 2015 made under the CHE project is shown in Figure 6.3. The CHE APO inventory was used by modellers to design a sampling strategy for additional tracers (CHE Deliverable 4.4 (D4.4 Sampling Strategy for additional tracers | CO2 Human Emissions (che-project.eu) but the inventory itself was not described in much detail. Although the same ORs were used in both products, the ambition for the CORSO regional APO inventory is to provide a more detailed inventory and a more complete description in CORSO in this deliverable. As can be seen in Figure 6.3, the CHE APO estimate for 2015 is around 3% lower than the new CORSO APO inventory. The drivers behind the higher O2 consumption in the CORSO product are the inclusion of the co-emitted species, and the more detailed fuel use for sea shipping

GridFED

The GridFED dataset provides a global inventory of anthropogenic APO, with a detailed description available in Section 5 (Jones et al., 2021). To facilitate a comparison between the datasets, a regional mask was applied to the GridFED data to extract CO2 emissions and O2 consumption specific to the European domain. This mask was created using a rectangular boundary, defined by latitude and longitude coordinates encompassing the region, including adjacent seas, from the North Atlantic Ocean to the European part of Russia, and from northern Greenland to southern Cyprus.

Comparing ORs between the two datasets required aligning their respective fuel types. While GridFED does not explicitly categorize emissions by sectors, it associates EDGAR activity sectors with its fuel categories (as outlined in Table 6.1). Given the differences in fuel definitions between GridFED (Jones et al., 2021) and the CAMS-based CORSO Regional APO product (Kuenen et al., 2022), direct comparisons were feasible only for coal, oil, gas, and shipping fuels.

Table 6.1: Relation of GCP-GridFED source classes to EDGAR activity sectors (Jones et al, 2021)

	GCP-GridFED Source Classes				
EDGAR Activity Sectors	**Oil**	**Natural Gas**	**Coal**	**Bunker Oil**	**Cement**
Power Industry	1A1a_OIL	1A1a_GAS	1A1a_COAL		
Fuel Transformation Industries	1A1b_1A1c_1A5b1_1B1b_1B2a5_1B2a6_1B2b5_2_C1b_OIL	1A1b_1A1c_1A5b1_1B1b_1B2a5_1B2a6_1B2b5_2_C1b_GAS	1A1b_1A1c_1A5b1_1B1b_1B2a5_1B2a6_1B2b5_2_C1b_COAL		
Manufacturing	1A2_OIL	1A2_GAS	1A2_COAL		
Buildings	1A4_OIL	1A4_GAS	1A4_COAL		
Transport: road	1A3b_OIL				
Transport: Rail, Pipelines, Off-Road	1A3c_1A3e (a)				
Fuel Exploitation	1B1a_1B2a1_1B2a2_1B2a3_1B2a4_1B2c_OIL	1B1a_1B2a1_1B2a2_1B2a3_1B2a4_1B2c_GAS			
Production of Iron and Steel			2C1a_2C1c_2C1d_2C1e_2C1f_2C2 (b)		
Production of Non-ferrous Metals			2C3_2C4_2C5 (b)		
Fossil Fuel Fires			7 A (c)		
Aviation	1A3a_CRS_domestic			1A3a_CRS_international	
(Cruising)	1A3a_CRS_domestic			1A3a_CRS_international	
Aviation (Landing and Take-Off)	1A3a_LTO_domestic			1A3a_LTO_international	
Aviation (Climbing & Descent)	1A3a_CDS_domestic			1A3a_CDS_international	
Shipping				1A3d_1C2 (d)	
Non-energy Use of Fuels	2 G (e)				
Solvents and Product Use	3 (f)				
Chemical Processes		2B (g)			
Non-metallic Minerals Production					2 A (h)

* while this table represents an earlier version of GridFED, the more recent GridFED version used for this comparison (version 2022) differentiates between bunker fuels for aviation and shipping, making the comparison with this fuel type possible.

As shown in Figure 6.7, O_2 consumption across both datasets generally follows similar trends, with key differences primarily driven by variations in CO_2 emissions. Although the CO_2 emissions reported by EDGAR and CAMS are relatively similar, they are not identical. These differences, which can occasionally exceed 10%, contribute to some discrepancies in CO_2 trends. Furthermore, the disparity in O_2 consumption is partly due to limitations in the mask used to extract information from GridFED. Because the domain extends to Russia, the rectangular mask includes several countries in the Middle East and Central Asia that are outside the CAMS domain. This inclusion results in higher reported CO_2 emissions and O_2 consumption.

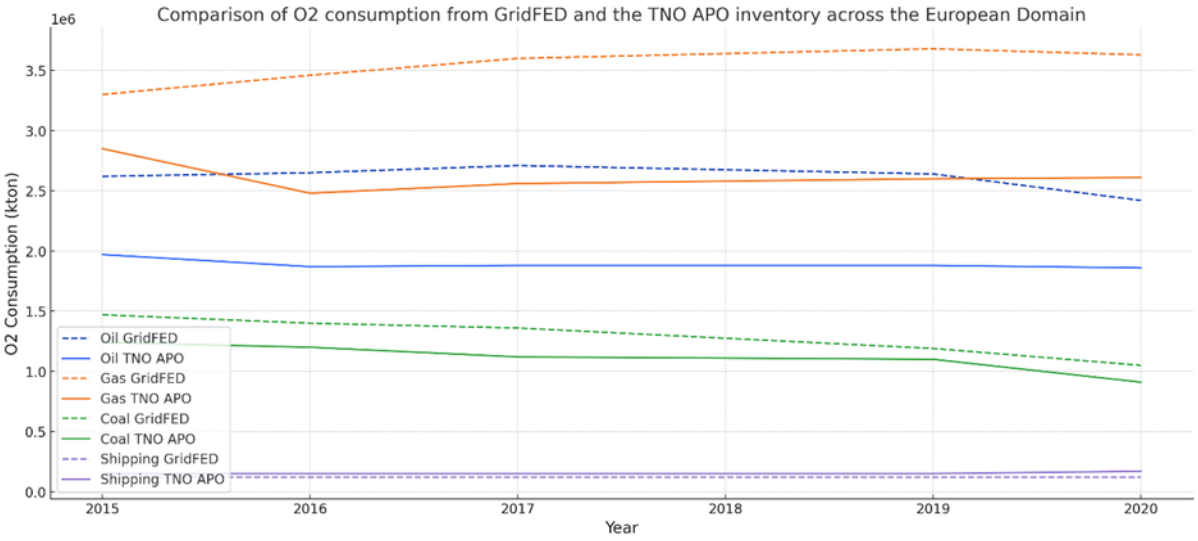

Figure 6.7: O_2 consumption per fuel type from GridFED and the regional TNO APO inventory across the European domain (2015-2020)

Moreover, the ORs across both datasets are nearly identical for Oil, Gas, and Coal. This similarity is expected, as the ORs in GridFED for these fuels are derived from Steinbach et al. (2011)'s COFFEE dataset, which is also the basis for the TNO APO inventory. The primary difference lies in the average OR for shipping. As discussed in Section 6.1.2, the TNO APO product employs a different methodology for shipping, which accounts for the higher O2 consumption, given that the years 2015-2020 had witnessed an increased use of LNG in sea shipping, resulting in a higher OR.

COFFEE

The CO2 release and Oxygen uptake from Fossil Fuel Emission Estimate (COFFEE) dataset provides a global view of CO2 emissions and O2 uptake from the combustion of various fossil fuels, combining high-resolution CO2 data from the EDGAR inventory with country-specific oxidative ratios. It features hourly global maps with 1°×1° resolution for 1996–2008 and examines the impact of these emissions on atmospheric oxygen levels and potential confusions with oceanic signals through model simulations and station observations (Steinbach et al., 2011).

The comparison of the COFFEE dataset with the TNO APO inventory, limited to the overlapping years of 2005–2008, reveals that the average OR is very similar across both products, as shown in Figure 6.8, with some variations. These differences arise from several factors. Firstly, the inclusion of distinct fuel types, such as cement in COFFEE, which is absent in the TNO inventory, and the adoption of a different methodology for OR calculation in sea shipping by the latter, contribute to the variations. Secondly, small discrepancies in CO_2 emissions between EDGAR and CAMS, combined with the impact of the regional mask used, also influence the overall average OR.

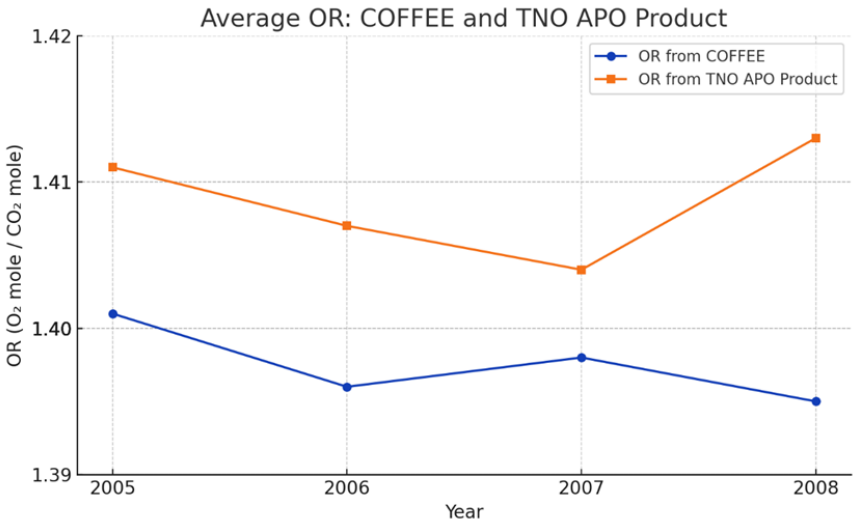

Figure 6.8: Timeseries comparison of the average ORs from 2005-2008 between the COFFEE inventory and the TNO APO inventory.

6.2. Data availability

The gridded dataset (0.05° x 0.1° resolution) is available to all project partners in NetCDF and CSV format on the following FTP repository:

CORSO

- Host: web-ftp81.tno.nl
- Protocol: FTP
- Encryption: Require explicit FTP over TLS
- Logon type: normal
- User: CORSO@ftp0015.web-ftp81
- Password: 4NVdConP4Yw7

See also Fig 6.9 for an overview of the directory structure.

CORSO

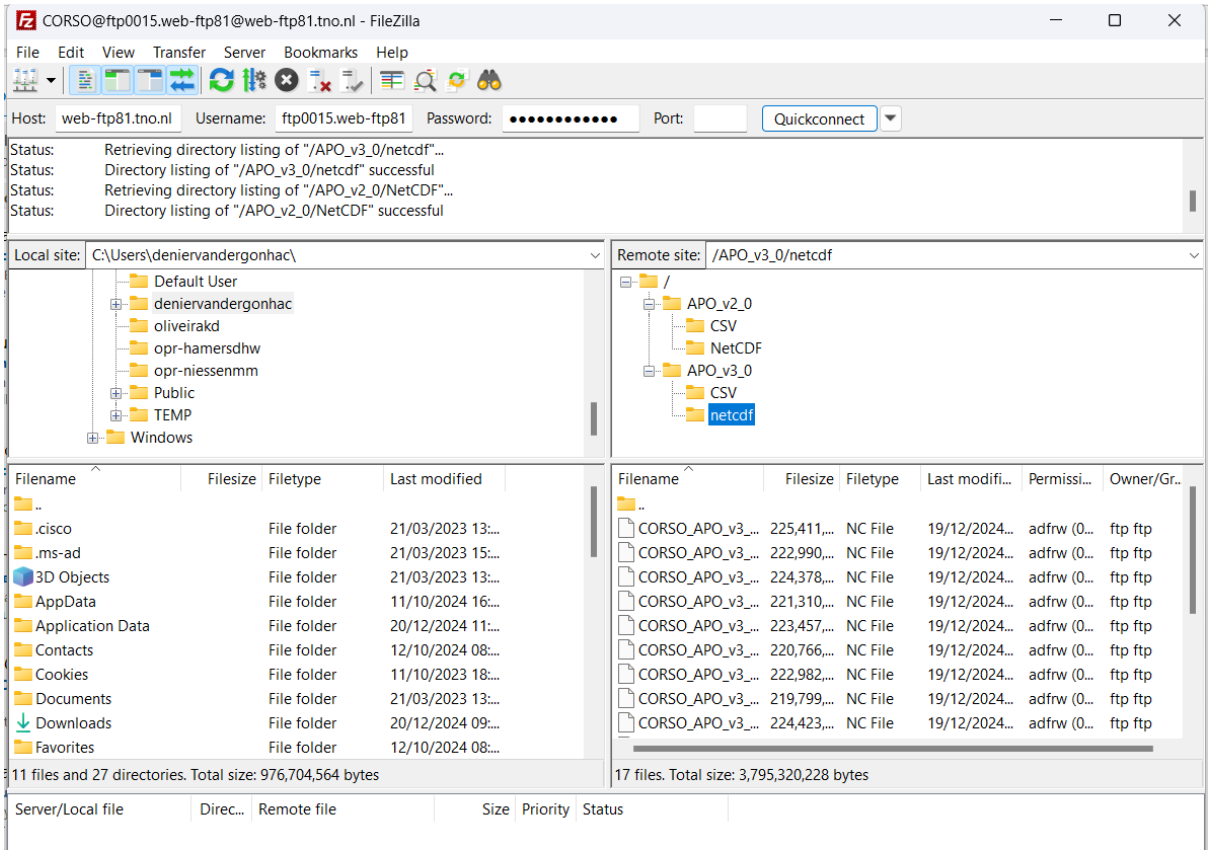

Figure 6.9: Screenshot showing the different APO versions on the TNO FTP server. APO-v2_0 was prepared for the CORSO milestone and covers 2005-2020. APO_v3_0 is the updated product described in this deliverable report and covers the period 2005-2023.

6.3. Contact Person(s)

TNO

Marya el Malki (marya.elmalki@tno.nl)

Hugo Denier van der Gon (hugo.deniervandergon@tno.nl)

6.4. References

Denier van der Gon, H., Gauss, M., Granier, C., Arellano, S., Benedictow, A., Darras, S., Dellaert, S., Guevara, M., Jalkanen, J.-P., Krueger, K., Kuenen, J., Liaskoni, M., Liousse, C., Markova, J., Prieto Perez, A., Quack, B., Simpson, D., Sindelarova, K., and Soulie, A.: Documentation of CAMS emission inventory products, https://atmosphere.copernicus.eu/node/1054, https://doi.org/10.24380/q2si-ti6i, 2023.

Jalkanen, J.-P., Johansson, L., and Kukkonen, J.: A comprehensive inventory of ship traffic exhaust emissions in the European sea areas in 2011, Atmos. Chem. Phys., 16, 71-84, https://doi.org/10.5194/acp-16-71-2016, 2016.

Johansson, L., J.-P. Jalkanen, and J. Kukkonen, Global assessment of shipping emissions in 2015 on a high spatial and temporal resolution, Atm. Env., 167, 403-415, doi: 10.1016/j.atmosenv.2017.08.042, 2017

Jones, M. W., Andrew, R. M., Peters, G. P., et al.: Gridded fossil CO_2 emissions and related O_2 combustion consistent with national inventories 1959–2018, Sci. Data, 8, 2, https://doi.org/10.1038/s41597-020-00779-6, 2021.

Kuenen, J., Dellaert, S., Visschedijk, A., Jalkanen, J.-P., Super, I., and Denier van der Gon, H.: CAMS[1]REG-v4: a state-of-the-art high-resolution European emission inventory for air quality modelling, Earth Syst. Sci. Data, 14, 491–515, https://doi.org/10.5194/essd-14-491-2022, 2022

Steinbach, J., Gerbig, C., Rödenbeck, C., Karstens, U., Minejima, C., and Mukai, H.: The CO_2 release and oxygen uptake from Fossil Fuel Emission Estimate (COFFEE) dataset: effects from varying oxidative ratios, Atmos. Chem. Phys., 11, 6855–6870, https://doi.org/10.5194/acp-11-6855-2011, 2011.

7. Future Scenarios

7.1. Introduction and motivation

In CORSO WP3, we address the question of the added value of $^{14}CO_2$ and APO observations in constraining fossil fuel CO_2 emissions. An important consideration is whether these indicators, which are valuable under present-day conditions, will remain valuable in the future with possibly different levels of CO_2 emission. For scenarios where fossil fuel CO_2 emissions continue to increase, this question can be easily answered based on findings from current concentration levels: if they work for present concentrations, they will also work for higher ones.

The key challenge, however, lies in determining whether these indicators remain sensitive enough under a scenario of declining fossil fuel CO_2 emissions. For this, we will select a scenario that reflects a reasonably optimistic outlook on fossil fuel emission reductions. The application of the outcomes of modelling with this scenario should flow into CORSO D3.5.

7.2. Scenario selection

We will select a scenario from the SSPs (Shared Socioeconomic Pathways) from IPCC Sixth Assessment Report (AR6) to construct emission products for the coming decades SSPs are climate change scenarios of projected socioeconomic global changes up to 2100, as defined in the IPCC AR6on climate change in 2021 (Figure 7.1).

Figure 7.1: Description of the five Shared Socioeconomic Pathways (SSPs) (O'Neill et al., 2017)

Of the five SSPs, SSP1 is the only scenario with decreasing fossil fuel CO_2 emissions between 2020 and 2050, making it our scenario of choice. This is illustrated in Figure 7.2.

Figure 7.2: Total CO2 emission for SSP1 (top) and SSP2 (bottom).

The blue line represents historic emissions, while the orange line depicts the SSP scenario prediction. SSP2 closely aligns with current emission trends, showing growing emissions towards 2050. In contrast, SSP1 shows a decreasing trend which is mostly linear between 2030 and 2090.

7.3. Methodology

The present-day GridFED APO grids (Jones et al., 2021) were chosen as a starting point for several reasons. Namely, they are already being used by WP3 in global simulations, they are readily available, and there is no suitable alternative without considerable additional work. The next step involved analysing the SSP1 scenario data and derive the necessary

information to scale the present-day GridFED data to the years 2030 and 2050. A simplified methodology scheme is shown in Figure 7.3.

Figure 7.3: Workflow to derive APO grid maps for future years (2030 and 2050) based on gridded GridFED APO data for the present (2019-2021).

The SSPs provide data for different stages of the energy chain. For the purpose of CORSO primary energy is the measure selected. Primary energy[1] is the most widely available statistic and very commonly used. Since APO depends on the fuel type used, the fuel type information contained in the SSP data is very important. The following types are provided in the SSPs: Coal, Gas, Oil, Biomass. Along with these, scenarios also contain information on Hydro, Nuclear, Solar, Wind and Non-Biomass Renewables but these are not used in our approach. The SSP energy data are only available for so-called world regions (Table 7.1).

Table 7.1: World regions as provided by the SSPs. The complete country list by region is in Appendix 7.1.

Region	**Definition**
OECD	Includes the OECD 90 and EU member states and candidates.
REF	Countries from the Reforming Economies of Eastern Europe and the Former Soviet Union.
ASIA	The region includes most Asian countries with the exception of the Middle East, Japan and Former Soviet Union states.
MAF	This region includes the countries of the Middle East and Africa.
LAM	This region includes the countries of Latin America and the Caribbean.

The next steps involved deriving scaling factors for each fuel type and region based on SSP1 data. Using 2020 as the base year, scaling factors were calculated by comparing forecasted CO_2 emissions under SSP1 to the 2020 values. The SSP1 data provide emissions estimates for five regions. To apply these scaling factors to GridFED, a mask was used to classify countries in the gridded data into the five regions defined by SSP1. Details of these regions and their classifications are provided in the Appendix of Chapter 7.

[1] Primary energy is the energy as it is available as resources – such as the fuels that are burnt in power plants –before it has been transformed. This relates to the coal before it has been burned; the uranium; or the barrels of oil.

7.4. Results

7.4.1. Scaling factors for future years relative to 2020

For every region, the same procedure is followed: the total energy consumption is taken from the SSPs IIASA database available at https://tntcat.iiasa.ac.at/SspDb. An example of the data is given in Figure 7.4. From this data we can calculate scaling factors by region by fuel type by taking the year 2020 as reference year (=1). The subsequent result for ASIA is shown in the lower panel of Figure 7.4. An example for a single fuel type (coal) for all regions is shown in Figure 7.5. The total set of scaling factors is shown in Table 7.2.

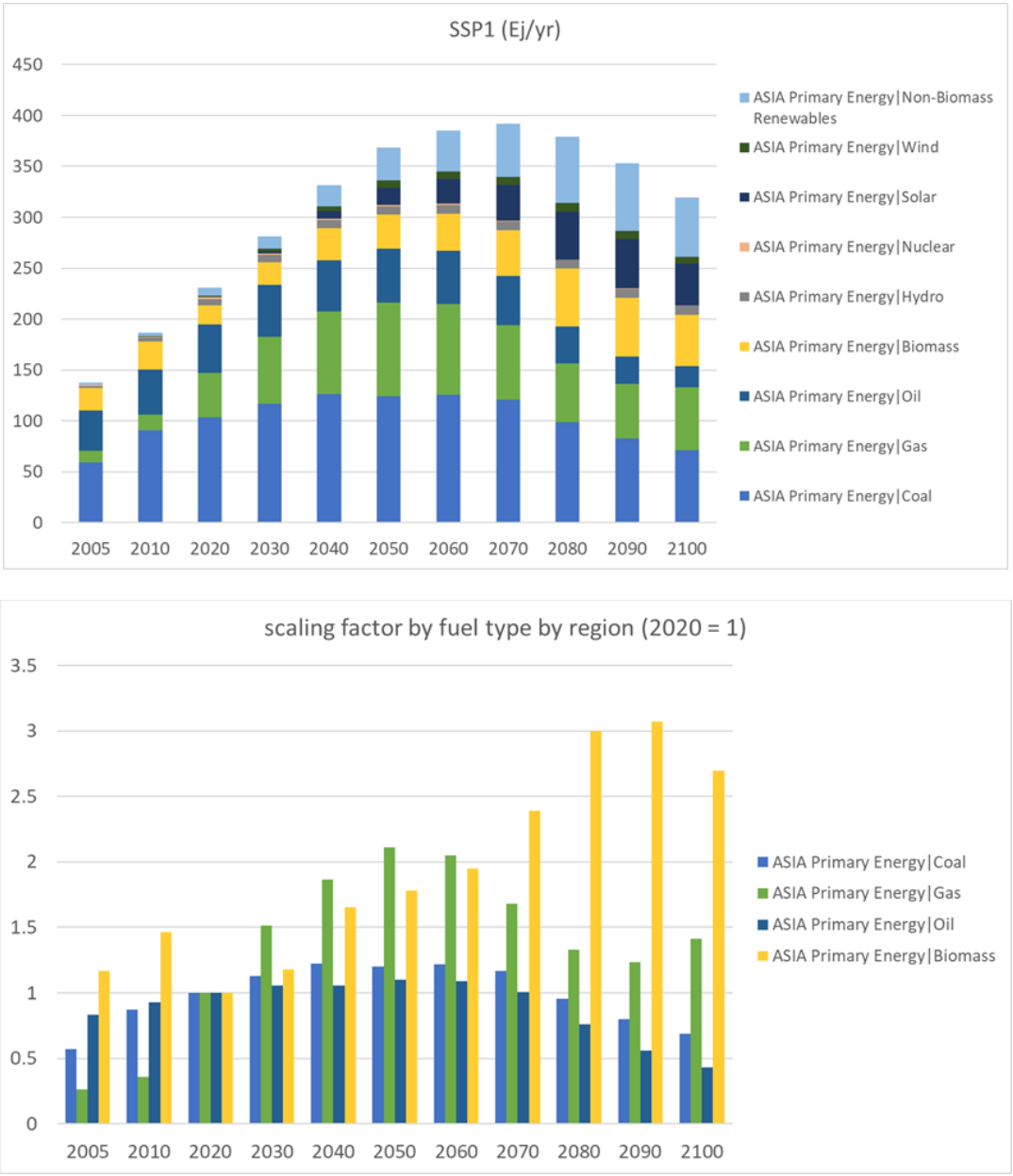

Figure 7.4: Example of the energy consumption data (Ej/yr) for SSP1 region Asia (top panel) and derived scaling factor relative to year 2020 (bottom panel). *Data source:* these figures are based on the SSP database hosted by the IIASA Energy Program at https://tntcat.iiasa.ac.at/SspDb.

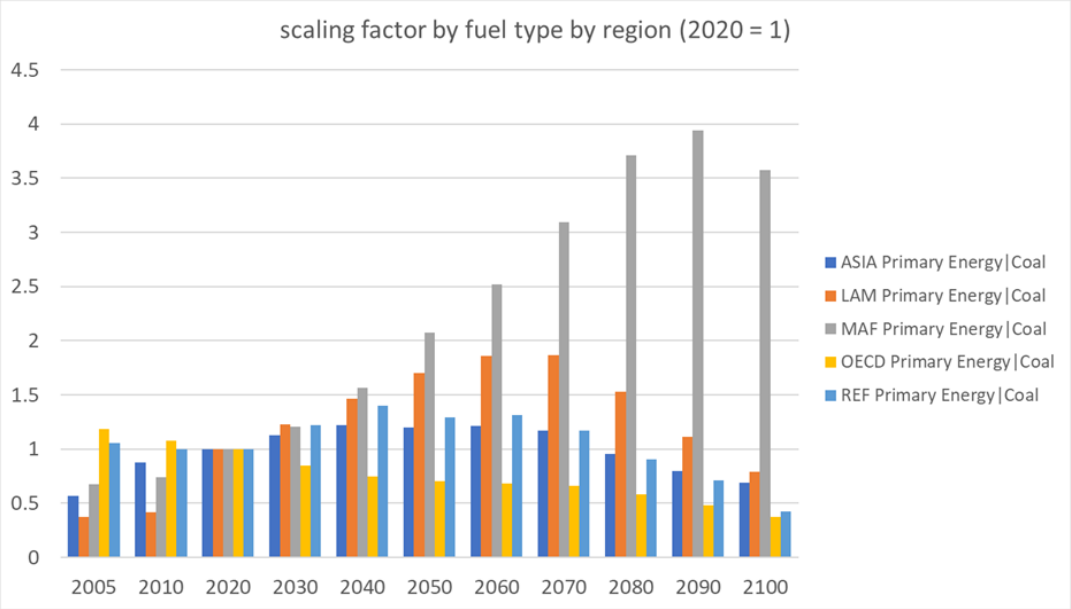

Figure 7.5: Example of the scaling factor relative to 2020 for energy consumption from coal following SSP1 for all five regions. Data source: These figures are based on the SSP database hosted by the IIASA Energy Program at https://tntcat.iiasa.ac.at/SspDb.

Table 7.2: Scaling factors based on the IMAGE model Scenario SSP1-Baseline energy consumption (2020 = 1). Original data source: SSP database hosted by the IIASA Energy Program at https://tntcat.iiasa.ac.at/SspDb , accessed November 2024.

Primary Energy	Region	2005	2010	2020	2030	2040	2050	2060	2070	2080	2090	2100
Coal	ASIA	0.57	0.87	1	1.13	1.22	1.2	1.22	1.17	0.96	0.8	0.69
Coal	LAM	0.38	0.42	1	1.23	1.47	1.7	1.86	1.87	1.53	1.11	0.79
Coal	MAF	0.68	0.74	1	1.21	1.57	2.07	2.52	3.09	3.71	3.94	3.57
Coal	OECD	1.18	1.08	1	0.85	0.75	0.7	0.68	0.66	0.58	0.48	0.37
Coal	REF	1.06	1	1	1.22	1.4	1.29	1.32	1.17	0.9	0.71	0.42
Gas	ASIA	0.26	0.36	1	1.52	1.86	2.11	2.05	1.68	1.33	1.23	1.41
Gas	LAM	0.52	0.61	1	1.51	1.96	2.15	2.18	2.01	1.71	1.47	1.27
Gas	MAF	0.7	0.87	1	1.37	2.06	2.86	3.78	4.25	4.24	3.97	3.61
Gas	OECD	0.9	0.93	1	1.22	1.43	1.35	1.35	1.34	1.3	1.25	1.22
Gas	REF	0.87	0.93	1	1.12	1.21	1.15	0.94	0.76	0.72	0.68	0.44
Oil	ASIA	0.83	0.93	1	1.05	1.06	1.1	1.09	1	0.76	0.56	0.43
Oil	LAM	0.87	0.91	1	0.95	0.86	0.93	0.97	0.78	0.45	0.29	0.22
Oil	MAF	0.68	0.78	1	1.15	1.23	1.25	1.25	1.29	1.15	0.83	0.61
Oil	OECD	1.23	1.09	1	0.73	0.54	0.48	0.41	0.3	0.21	0.17	0.14
Oil	REF	1.13	1.04	1	0.87	0.55	0.48	0.45	0.43	0.36	0.35	0.32

7.4.2. GridFED-based APO data for future years

The gridded data constructed under CORSO Task 3.2.4 provides a time-series analysis of changes in CO_2 emissions and O_2 consumption from 2020 (the base year) to 2100, based on the fossil fuel reduction scenario defined under SSP1. As illustrated in Figures 7.6 and 7.7, this scenario leads to significant reductions in CO_2 emissions and, consequently, O_2 consumption from oil and coal.

For oil (Figure 7.6), little change is observed in 2030 for most regions, with minor decreases in LAM (-5%) and REF (-13%), while ASIA and MAF show slight increases of 5% and 15%, respectively. However, a substantial reduction of 30% is observed in the OECD. By 2050, CO_2 emissions in the OECD and REF regions have already been cut by more than half (-52% each), whereas emissions in ASIA and MAF continue to rise, peaking in 2060 and 2070, respectively.

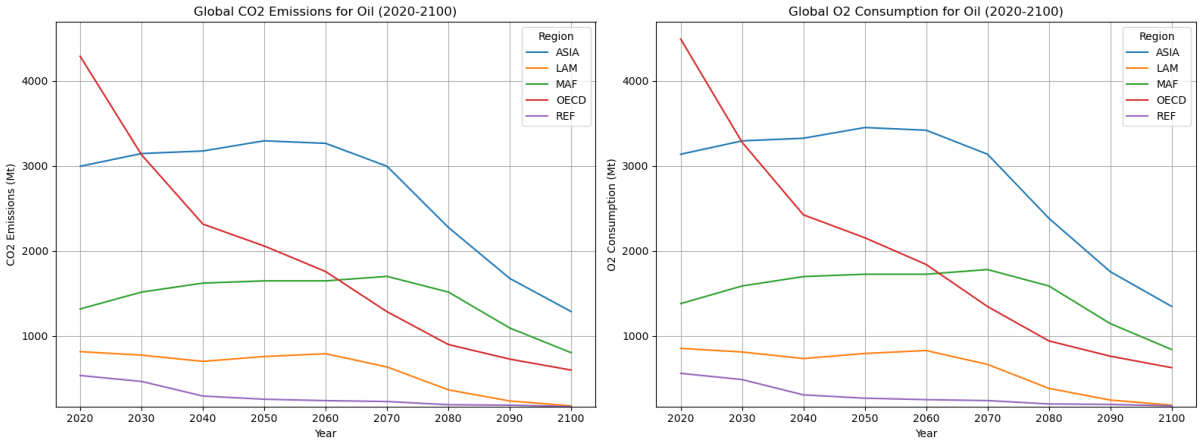

Figure 7.6: Global CO_2 Emissions (Mt) and O_2 Consumption (Mt) from Oil under SSP1 from 2020 (base-year) to 2100

For coal (Figure 7.7), emissions increase in all regions except the OECD by 2030. By 2050, reductions are observed in LAM and REF, while MAF continues to rise until peaking in 2090. ASIA, which is by far the largest contributor to CO_2 emissions from coal—three times the cumulative emissions from all other regions—remains above 2020 levels until around 2080.

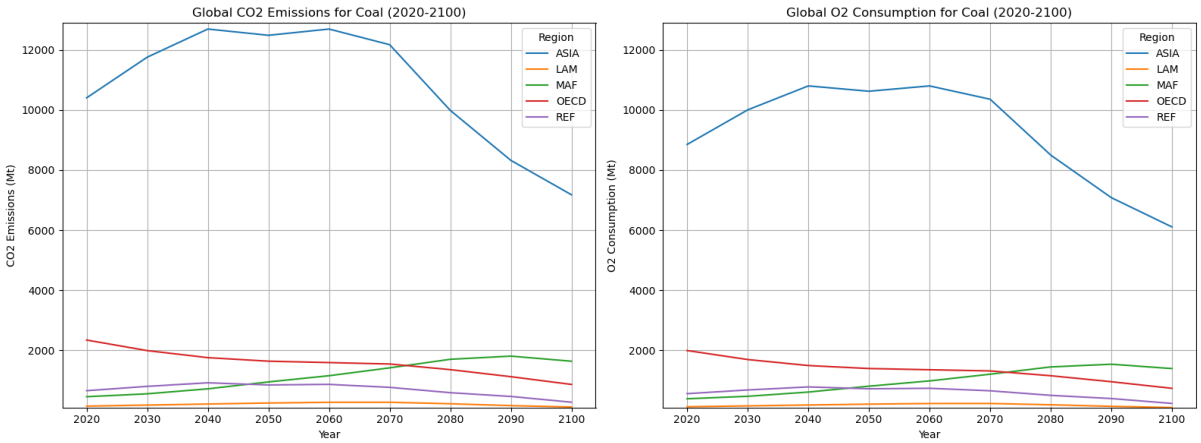

Figure 7.7: Global CO_2 Emissions (Mt) and O_2 Consumption (Mt) from Coal under SSP1 from 2020 (base-year) to 2100

Regarding gas, emissions increase in both 2030 and 2050 compared to 2020. Since the phase-out of gas under SSP1 is slower than that of oil and coal, most regions continue to

show higher emissions compared to 2020 in 2100. However, by then, emissions begin to decline from their peaks.

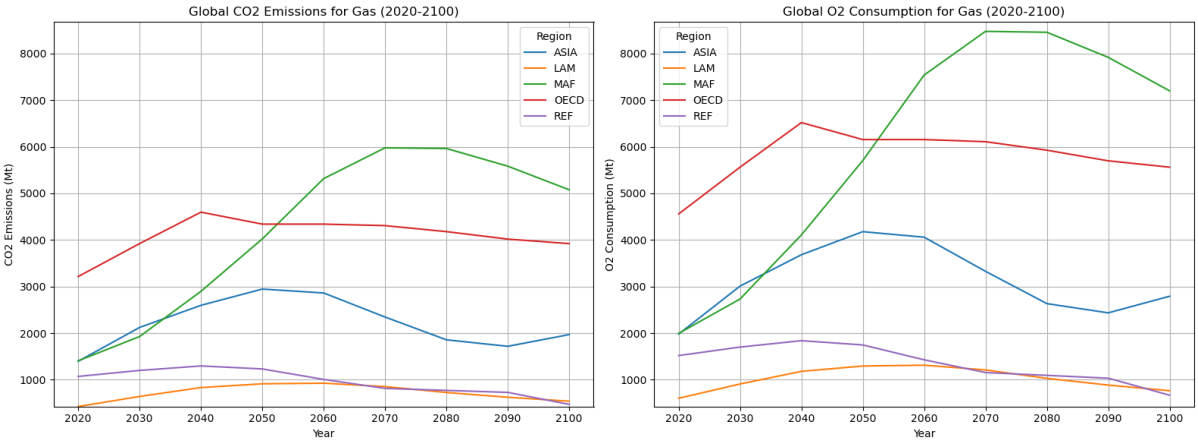

Figure 7.8: Global CO_2 Emissions (Mt) and O_2 Consumption (Mt) from Gas under SSP1 from 2020 (base-year) to 2100

Overall, this analysis demonstrates that under a fossil fuel reduction scenario like SSP1, CO_2 emissions and, consequently, O_2 consumption generally decrease, though with significant variation across fuel types and regions. These findings enable further investigation into the sensitivity of APO as a tracer for future CO_2 emissions, particularly in the context of drastic global reductions in anthropogenic CO_2 emissions over the coming decades.

7.5. Data Availability

The gridded dataset (0.1° x 0.1° resolution) is available from 15 February 2025 onwards to all project partners in NetCDF and CSV format on the following TNO FTP repository:

CORSO

- Host: web-ftp81.tno.nl
- Protocol: FTP
- Encryption: Require explicit FTP over TLS
- Logon type: normal
- User: CORSO@ftp0015.web-ftp81
- Password: 4NVdConP4Yw7

7.6. Contact persons

TNO

Marya el Malki (marya.elmalki@tno.nl)

Hugo Denier van der Gon (hugo.deniervandergon@tno.nl)

7.7. References

Jones, M. W., Andrew, R. M., Peters, G. P., et al.: Gridded fossil CO_2 emissions and related O_2 combustion consistent with national inventories 1959–2018, Sci. Data, 8, 2, https://doi.org/10.1038/s41597-020-00779-6, 2021.

IIASA: SSP database hosted by the IIASA Energy Program, available at: https://tntcat.iiasa.ac.at/SspDb, last access: November 2024.

O’Neill, B. C., Kriegler, E., Ebi, K. L., Kemp-Benedict, E., Riahi, K., Rothman, D. S., van Ruijven, B. J., van Vuuren, D. P., Birkmann, J., Kok, K., Levy, M., and Solecki, W.: The roads ahead: Narratives for shared socioeconomic pathways describing world futures in the 21st century, Glob. Environ. Change, 42, 169–180, https://doi.org/10.1016/j.gloenvcha.2015.01.004, 2017.

Appendix 7.1: Countries included in the five regions used in the SSP

OECD = Includes the OECD 90 and EU member states and candidates.
Albania, Australia, Austria, Belgium, Bosnia and Herzegovina, Bulgaria, Canada, Croatia, Cyprus, Czech Republic, Denmark, Estonia, Finland, France, Germany, Greece, Guam, Hungary, Iceland, Ireland, Italy, Japan, Latvia, Lithuania, Luxembourg, Malta, Montenegro, Netherlands, New Zealand, Norway, Poland, Portugal, Puerto Rico, Romania, Serbia, Slovakia, Slovenia, Spain, Sweden, Switzerland, The former Yugoslav Republic of Macedonia, Turkey, United Kingdom, United States of America

REF = Countries from the Reforming Economies of Eastern Europe and the Former Soviet Union.
Armenia, Azerbaijan, Belarus, Georgia, Kazakhstan, Kyrgyzstan, Republic of Moldova, Russian Federation, Tajikistan, Turkmenistan, Ukraine, Uzbekistan

ASIA = The region includes most Asian countries with the exception of the Middle East, Japan and Former Soviet Union states.
Afghanistan, Bangladesh, Bhutan, Brunei Darussalam, Cambodia, China (incl. Hong Kong and Macao, excl. Taiwan) Democratic People's Republic of Korea, Fiji, French Polynesia, India, Indonesia, Lao People's Democratic Republic, Malaysia, Maldives, Micronesia (Fed. States of), Mongolia, Myanmar, Nepal, New Caledonia, Pakistan, Papua New Guinea, Philippines, Republic of Korea, Samoa, Singapore, Solomon Islands, Sri Lanka, Taiwan, Thailand, Timor-Leste, Vanuatu, Viet Nam

MAF = This region includes the countries of the Middle East and Africa.
Algeria, Angola, Bahrain, Benin, Botswana, Burkina Faso, Burundi, Cameroon, Cape Verde, Central African Republic, Chad, Comoros, Congo, Côte d`Ivoire, Democratic Republic of the Congo, Djibouti, Egypt, Equatorial Guinea, Eritrea, Ethiopia, Gabon, Gambia, Ghana, Guinea, Guinea-Bissau, Iran (Islamic Republic of), Iraq, Israel, Jordan, Kenya, Kuwait, Lebanon, Lesotho, Liberia, Libyan Arab Jamahiriya, Madagascar, Malawi, Mali, Mauritania, Mauritius, Mayotte, Morocco, Mozambique, Namibia, Niger, Nigeria, Occupied Palestinian Territory, Oman, Qatar, Rwanda, Réunion, Saudi Arabia, Senegal, Sierra Leone, Somalia, South Africa, South Sudan, Sudan, Swaziland, Syrian Arab Republic, Togo, Tunisia, Uganda, United Arab Emirates, United Republic of Tanzania, Western Sahara, Yemen, Zambia, Zimbabwe

LAM = This region includes the countries of Latin America and the Caribbean.
Argentina, Aruba, Bahamas, Barbados, Belize, Bolivia (Plurinational State of), Brazil, Chile, Colombia, Costa Rica, Cuba, Dominican Republic, Ecuador, El Salvador, French Guiana, Grenada, Guadeloupe, Guatemala, Guyana, Haiti, Honduras, Jamaica, Martinique, Mexico, Nicaragua, Panama, Paraguay, Peru, Suriname, Trinidad and Tobago, United States Virgin Islands, Uruguay, Venezuela (Bolivarian Republic of)

8. Conclusion

This document represents the completion of Deliverable D3.4 for CORSO's Work Package 3, Task 3.2. It reflects the collaborative effort in developing comprehensive datasets, documenting methodologies, and presenting findings detailed to support further research and applications in the CORSO project. Each chapter provides an overview of a dataset, the contact persons and how to access the data.

The final CORSO Task 3.2 deliverable includes expanded datasets for oceanic and terrestrial 14CO2 fluxes, nuclear power plants, oceanic APO products, global and regional anthropogenic APO products and future scenarios for APO. Users are encouraged to explore these resources and are welcome to reach out using the provided contact details for any additional information or discussions.

Document History

Version	Author(s)	Date	Changes
0.1	Marya el Malki, Hugo Denier van der Gon, Hannah Allen, Grégoire Broquet, Carlos Gomez, Marko Scholze, Eric Saboya, Philippe Ciais, Claire Granier, Antoon Visschedijk	Dec 2024	Initial version
0.2	Hugo Denier van der Gon	Jan 2025	Minor update
1.0	Marya el Malki, Hugo Denier van der Gon, Hannah Allen, Grégoire Broquet, Carlos Gomez, Marko Scholze, Eric Saboya, Philippe Ciais, Claire Granier, Antoon Visschedijk	Feb 2025	Issued revised version after processing review comments
1.1	Marya el Malki, Hugo Denier van der Gon, Marko Scholze	Feb 2025	Minor update regarding data availability

Internal Review History

Internal Reviewers	Date	Comments
Richard Engelen, ECMWF and Harro Meijer RUG	Jan 2025	Provided as comments in the submitted report version 0.2